M.Tech (Power Electronics and Systems)

Dhananjay Yadav

2023

CAPACITOR TRAPPED CURRENT FED SOFT SWITCHING PUSH PULL DC-DC CONVERTER FOR RENEWABLE ENERGY CONVERSION

A DISSERTATION

SUBMITTED IN PARTIAL FULFILLMENT OF THE REQUIREMENTS

FOR THE AWARD OF THE DEGREE

OF

MASTER OF TECHNOLOGY

IN

POWER ELECTRONICS AND SYSTEMS

Submitted by:

DHANANJAY YADAV

2K21/PES/07

Under the supervision of

PROF. VISHAL VERMA

(Professor, EED, DTU)

DEPARTMENT OF ELECTRICAL ENGINEERING
DELHI TECHNOLOGICAL UNIVERSITY
(Formerly Delhi College of Engineering)
Bawana Road, Delhi-110042

MAY, 2023

DEPARTMENT OF ELECTRICAL ENGINEERING

DELHI TECHNOLOGICAL UNIVERSITY

(Formerly Delhi College of Engineering)

Bawana Road, Delhi-110042

CANDIDATE'S DECLARATION

I, Dhananjay Yadav, Roll No. 2K21/PES/07 student of MTech (Power Electronics & Systems), hereby declare that the project Dissertation titled **"Capacitor Trapped Current fed Soft Switching Push Pull DC-DC Converter for Renewable Energy Conversion "** which is submitted by me to the Department of Electrical Engineering, Delhi Technological university, Delhi in partial fulfilment of the requirement for the award of the degree of Master of Technology, is original and not copied from any source without proper citation. This work has not previously formed the basis for the award of any Degree, Diploma Associateship, Fellowship or other similar title or recognition.

Place: Delhi (Dhananjay Yadav)

Date: 31/05/23

DEPARTMENT OF ELECTRICAL ENGINEERING

DELHI TECHNOLOGICAL UNIVERSITY

(Formerly Delhi College of Engineering)

Bawana Road, Delhi-110042

CERTIFICATE

I hereby certify that the project Dissertation titled **"Capacitor Trapped Current fed Soft Switching Push Pull DC-DC Converter for Renewable Energy Conversion"** which is submitted by Dhananjay Yadav, Roll No. 2K21/PES/07, Department of Electrical Engineering, Delhi Technological University, Delhi in partial fulfilment of the requirement for the award of the degree of Master of Technology, is a record of the project work carried out by the student under my supervision. To the best of my knowledge this work has not been submitted in part or full for any Degree or Diploma to this University or elsewhere.

Place: Delhi
Date: 31/05/23

PROF. VISHAL VERMA
(SUPERVISOR)

ABSTRACT

The design and analysis of Capacitor Trapped Current fed Soft Switching Push Pull DC-DC Converters for renewable energy conversion applications is presented in this thesis work. The proposed two converters are designed to address the challenges of efficient power conversion and integration of renewable energy sources by combining the inherit advantages of current fed push pull converter with ZCS technique to achieve high efficiency, lower conduction losses of the primary switches , low EMI noise , high reliability and smaller size. The nominal 48V bus voltage is step up to 380V utilizing the proposed converters operating at 100kHz switching frequency and 500W power level. The first architecture uses dual trapped capacitor structure on the primary side to achieve ZCS and the second architecture uses single capacitor trapped structure to achieve ZCS owing to the resonance between the primary side trapped capacitors and leakage inductance of the HF transformer as a result the first architecture is able to achieve voltage at transformer's primary having quasi square waveform and sinusoidal waveform in case of secondary architecture. In both proposed architectures natural clamping is achieved which results in mitigating the need of auxiliary clamping or snnuber circuit to reduce voltage stress on power switches as a result number of requirement of power switches also reduces. The voltage spike across the power devices are suppressed effectively enabling the selection of low voltage, low cost power devices. Since all the switches are ground referred in both proposed converters, non-isolated driver with single power supply can be employed. SiC diodes are used in the output rectifier side to minimize to reverse recovery problem in both the proposed architectures.

DEPARTMENT OF ELECTRICAL ENGINEERING

DELHI TECHNOLOGICAL UNIVERSITY

(Formerly Delhi College of Engineering)

Bawana Road, Delhi-110042

ACKNOWLEDGEMENT

I would like to express my gratitude towards all the people who have contributed their precious time and effort to help me without whom it would not have been possible for me to understand and complete the project. I would like to thank Prof. Vishal Verma, DTU Delhi, Department of Electrical Engineering, my Project Supervisor, for supporting, motivating and encouraging me throughout the period of this work was carried out. His readiness for consultation at all times, his educative comments, his concern and assistance even with practical things have been invaluable.

Besides my supervisor, all the PhD scholars of my LAB for helping me wherever required and provided me continuous motivation during my research.

Finally, I must express my very profound gratitude to my parents, seniors and to my friends for providing me with unfailing support and continuous encouragement throughout the research work.

Date: 31/05/23

Dhananjay Yadav
M.tech (Power Electronics & Systems)
Roll No. 2K21/PES/07

TABLE OF CONTENTS

LIST OF TABLES

LIST OF FIGURES

LIST OF ABBREVIATION

PV	Photovoltaic
DC	Direct Current
IRENA	International Renewable Energy Agency
IPCC	Intergovernmental Panel on Climate Change
SDG	Sustainable Development Goals
MPPT	Maximum Power Point Tracking
HF	High Frequency
PP	Push-Pull
ZVS	Zero Voltage Switching
ZCS	Zero Current Switching
SiC	Silicon Carbide
UPS	Uninterruptible Power Supply
EV	Electric Vehicle
RCD	Resistor Capacitor Diode
EMI	Electromagnetic Interference
FB	Full Bridge

LIST OF SYMBOLS

V_{IN}	Input Voltage to the Converter
I_{IN}	Input current to the Converter
N_P	Number of Primary Turns in Transformer
N_s	Number of secondary Turns in Transformer
V_O	Output Voltage of the Converter
V_{S1}	Voltage across Switch S1
V_{S2}	Voltage across Switch S2
V_{LIN}	Voltage across Input Inductor
D	Duty Cycle
$V_{C1\ trapped}$	Voltage across Trapped Capacitor C1
$V_{C2\ trapped}$	Voltage across Trapped Capacitor C2
I_{OUT}	Output Current of the Converter
L_{TF}	Total Leakage Inductance of Transformer's Primary
$I_{C1\ trapped}$	Current through Trapped Capacitor C1
$I_{C2\ trapped}$	Current through Trapped Capacitor C2
n	Transformer's Number of Turns
w_o	Resonant Frequency
T_s	Switching Period

CHAPTER 1
INTRODUCTION

1.1 Background

The world is facing significant challenges related to energy generation, consumption, and environmental sustainability. The production, use, and sustainability of energy are important issues in the global community. As the negative impacts of fossil fuel-based energy sources have become more and more obvious, there is an urgent need to move to renewable energy systems. Solar, wind, hydro, and geothermal renewable energy sources have enormous potential for the production of clean and sustainable energy. However, to harness and integrate this abundant resource into the current power grid, the use of renewable energy requires efficient and reliable conversion technologies. This section explores the need for renewable energy conversion systems and highlights the latest data on renewable energy, to emphasize the urgency of this transition.

1. **Global Energy Scenario –** The existing energy landscape is largely based on fossil fuels, which not only contribute to greenhouse gas emissions but also deplete natural resources. The International Energy Agency (IEA) estimated that 80% of the world's energy consumption in 2022 originated from fossil fuels, which hastens global warming, air pollution, and geopolitical tensions. The environment and welfare of people are significantly at risk owing to this dependency on non-renewable energy sources.
2. **Environmental Concerns and Climate Change –** Climate change, which is one of the most urgent problems of our day, is principally caused by excessive carbon dioxide emissions from burning fossil fuels. The Intergovernmental Panel on Climate Change (IPCC) issues a dire warning that, to prevent catastrophic effects, immediate action must be taken to keep global warming far below 2 °C above pre-industrial levels. Greenhouse gas emissions can be reduced and climate change can be mitigated by using renewable energy sources.

3. **Growing Renewable Energy Capacity –** In the last ten years, the implementation of renewable energy has advanced remarkably. In 2020 alone, there were nearly 500 GW of new installations for renewable energy according to the Renewable Energy Market Update 2021 by the International Renewable Energy Agency (IRENA). As solar and wind energy become more affordable, they are being used more frequently and are advancing technologically. The shift to renewable energy systems has sped up as a result of favorable legislation, falling costs of renewable energy technology, and rising public awareness.
4. **Energy Security and Independence -** Systems for converting renewable energy are essential for improving energy independence and security. In contrast to fossil fuels, renewable energy sources are plentiful and widely dispersed, which lessens the dependency on imported energy sources. Utilizing local resources helps countries with significant renewable energy potential increase their energy independence and reduce their vulnerability to price swings and geopolitical conflicts brought about by the import of fossil fuels.
5. **Economic Opportunities and Job Creation -** The renewable energy industry has become a vital engine for economic expansion and job development. Over 11.5 million people were employed globally in the renewable energy sector in 2019, according to the International Renewable Energy Agency (IRENA). There is huge potential for job growth as the industry develops, particularly in the production, installation, operation, and maintenance of renewable energy systems. The advancement of renewable energy technology can also encourage innovation, research, and development, thereby enhancing both sustainable development and economic competitiveness.
6. **Sustainable Development Goals –** The Sustainable Development Goals (SDGs) of the United Nations offer a thorough framework for international development, including SDG 7's promotion of clean, affordable energy for all. Several SDGs, including eradicating poverty, enhancing health, guaranteeing access to clean water and sanitation, and halting climate change, depend heavily on renewable energy systems. Countries can make major strides towards accomplishing these objectives and building a more sustainable and equitable future by adopting renewable energy conversion technologies.

Systems for converting renewable energy are now more essential than ever. To combat climate change, reduce greenhouse gas emissions, improve energy security, stimulate economic growth, and advance sustainable development, it is imperative to switch to renewable energy sources. Recent information on renewable energy emphasizes the explosive expansion and enormous potential of this industry. Governments, companies, and individuals must work together to speed up the adoption of renewable energy conversion systems and build a sustainable energy future for future generations.

1.2 Need of DC-DC Converter for renewable energy Conversion

Alternatives to conventional fossil fuel based power generation, such as solar photovoltaic (PV) and wind turbines, are clean and sustainable. However, advanced power electronics systems are required for the efficient conversion, integration, and use of renewable energy. Solar energy being abundant and closest to the loading point, but struggle with intermittency issues and generally yield low output voltages, and thus require step-up DC-DC converters having high conversion ratio with low input current ripple for its effective utilization for off grid and grid connected application [1][8]. In particular, the use of DC-DC converters in renewable energy conversion systems is essential. The importance of DC-DC converters in easing the conversion and integration of renewable energy sources is examined in this section, which also highlights the importance of maximizing the energy efficiency and enabling the widespread adoption of renewable energy technology.

1. **Variable Output of Renewable Energy Sources –** Owing to changes in climatic conditions, renewable energy systems, such as solar PV and wind turbines, provide electricity with variable voltage and power characteristics. Wind turbines produce AC power at various frequencies and voltages, whereas solar photovoltaic (PV) systems produce DC power. It is crucial to convert and control the generated power to fit the demands of the load or grid to effectively use this variable energy output. In these energy conversion processes, DC-DC converters are essential because they allow for accurate and efficient regulation of power flow, voltage levels, and compatibility of various energy system components.
2. **Voltage Conversion and Integration with the Grid** - The voltage levels at which renewable energy sources frequently provide power are different from

those required by the grid or by the loads. DC-DC converters make voltage conversion easier by increasing or decreasing the voltage levels to meet grid or load requirements. With these voltage conversion capabilities, renewable energy sources can be seamlessly integrated into the current power infrastructure to facilitate effective energy transfer and utilization. In addition, DC-DC converters include isolation, protection, and control features that improve the stability and dependability of the system for converting renewable energy.

3. **Maximum Power Point Tracking (MPPT) -** Obtaining the maximum power possible from a renewable energy source is one of the most significant challenges, particularly for solar PV systems. Temperature and incident solar radiation have a significant impact on the output power of solar panels. Maximum Power Point Tracking (MPPT), an advanced control technique for DC-DC converters, allows for real-time monitoring and adjustment of the operating point of a renewable energy source. This guarantees that the system works at the point when the maximum power can be extracted, thereby improving the total energy efficiency and yield of the system.

4. **Energy Storage Integration -** The intermittency and unpredictability of renewable energy sources are addressed by energy storage technologies, such as batteries [9], which are essential components of renewable energy systems. By managing the power flow between the renewable energy source, storage system, and load, DC-DC converters enable the effective charging and discharging of energy storage systems. As a result, effective energy management, peak shaving, and grid stabilization were made possible. The efficiency and resilience of the system as a whole are increased by using DC-DC converters to enable the best possible energy conversion and transfer between the storage system and renewable energy source.

5. **System Efficiency and Power Quality -** In systems for converting renewable energy, DC-DC converters have a considerable impact on the overall system efficiency and power quality. The efficiency of the system as a whole is increased by efficient power conversion, which reduces energy losses during the conversion process. In addition, voltage regulation, and harmonic suppression are made possible by DC-DC converters, ensuring good power

quality and grid compatibility. Power electronic components and sophisticated control algorithms have been combined to improve the performance, efficiency, and reliability of DC-DC converters. Fig. 1.1 shows a block diagram of the architecture of a renewable energy conversion system.

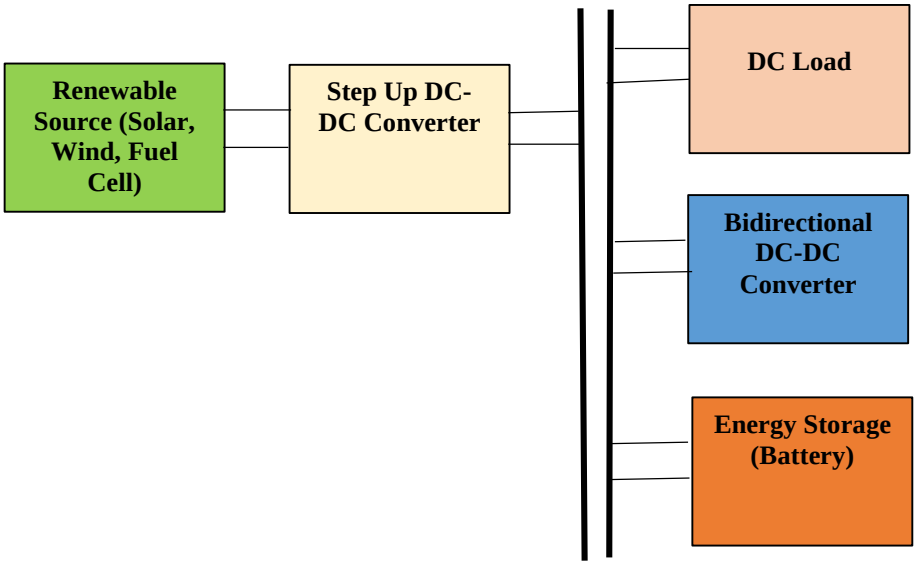

Fig. 1.1 Block Diagram of Architecture of Renewable Energy Conversion System

DC-DC converters can be categorized into two types i.e. either isolated or non-isolated, however, the isolated converters with High-frequency (HF) transformer are chosen over non-isolated topologies because of their advantages in galvanic isolation, low ripple contents, enhanced regulation, flexible output voltage, and provide multiple output at different levels with ease. Electrical isolation between the input and output reduces the risk of electrical shock and protect the delicate components against ground events, and electrical noise.

Current fed converters are considered front runner in various step-up dc-dc converters applicable to PV fed system. These converters naturally come with smaller input current pulsations and due to pre-boosting paving the advantage of a lower transformer turns ratio compared to voltage-fed converters with output voltage clamping, risks of HF transformer getting saturated reduced largely and there are no duty cycle loss issues. Therefore, current-fed DC-DC converters are preferred over voltage-fed counterparts for applications converting low voltage renewable energy sources [2].

For isolated current-fed step-up DC-DC converters, the most popular topologies include flyback, half-bridge, full-bridge, and push-pull (PP) architectures. For galvanic isolation initially line frequency (50–60 Hz) transformers [3] are employed, although dependable and simple, its large size and weight is major impediment. Flyback converter falter on account of large losses and significant voltage drop as the step up voltage output increases. On the other hand, the half-bridge converter architecture falls short for high step up applications when compared to the PP or full-bridge converter arrangement since it needs double the turn ratio of the equivalent HF transformer. Features like simple circuitry, fewer power switches, reduced conduction losses, high step up voltage conversion ratio, better transformer utilization makes the PP converter more suitable as compared to full bridge configurations. Owing to utilization of the leakage inductor of the HF transformer as integrated magnetic solution, the power density is increased drastically for energy transfer in current-fed topologies [3].

Traditional current-fed push-pull converters have a number of drawbacks, such as high voltage spikes across switches brought owing to resonance between the switching loop parasitic capacitor and the HF transformer's leakage inductance, and high switching losses owing to the primary switches hard switching operation. Passive snubbers, energy recovery circuits, and active clamp snubbers are reported in the literature [3] to provide protection against high spikes on the switches. Active-clamp snubbers are favorably utilized as their auxiliary circuit may not only suppressed the voltage spikes but also assisted in zero voltage switching (ZVS) thereby showing high efficiency hence, paving the way for increase in the switching frequency and reduction of the converter size[4]. For further effective remediation, numerous enhanced topologies with ZVS [3], zero current switching (ZCS) [4], and voltage spike clamping and suppression [4] are suggested in literature. The resonant push-pull converters, which use the circuit parasitic, or resonant tank to help with ZVS or ZCS for primary switches, is also reported [5].These methods achieve a high conversion efficiency while reducing the switching loss drastically.

1.3 Thesis Objectives

The objective of this thesis is to design, analyze, and evaluate a highly efficient, low EMI, light weight, low cost, high power density, highly reliable, current fed push-pull converter to address the challenges associated with efficient power conversion and

integration of renewable energy sources into the grid by utilizing the advantages offered by the current fed push-pull topology combined with ZCS operation. The work done in the thesis is primarily focused on providing higher efficiency , lower cost and easy to implement current fed push pull converter circuit with trapped clamping capacitor in the primary side to achieve natural clamping. Effective suppression of the voltage spike across the power devices enables the selection of low voltage, low cost power devices. Since all the switches are ground referred, non-isolated driver with single power supply can be employed with simple control. The novel topology helps in achieving ZCS owing to the resonance between the trapped capacitor and the leakage inductance of the HF transformer, resulting in a near sinusoidal waveform at the primary of the HF transformer.

Overall, this thesis aims to contribute to the advancement of current fed push-pull converters with ZCS technique for renewable energy conversion. The findings and insights gained from this research can enhance the efficiency, performance, and reliability of renewable energy systems, supporting the broad adoption and integration of renewable energy sources into the existing power infrastructure.

1.4 Structural Organization of the thesis

This thesis is organized as follows:

1. **Chapter 1** explains the need for a DC-DC converter and its relevance to renewable energy conversion applications.
2. **Chapter 2** provides an extensive review regarding current fed push-pull converters in order to cover various aspects such as design principles, control strategies, and techniques employed to improve their efficiency. The literature on this topic is thoroughly reviewed to offer a comprehensive understanding.
3. **Chapter 3** focuses on the design and modelling of the conventional current fed push-pull converter, including the mathematical analysis and MATLAB simulation results explained in detail.
4. **Chapter 4** centers around the design and modeling of the dual capacitor trapped ZCS current fed push-pull converter, with a detailed explanation of the mathematical analysis and MATLAB simulation results provided. The chapter delves into the intricacies of this converter and presents a comprehensive

exploration of its design principles and simulation outcomes.

5. **Chapter 5** investigates and implements a capacitor trapped ZCS current fed push-pull converter, and the usage of SiC diodes at the output rectifier side. The experimental validation of the proposed Capacitor trapped ZCS push pull DC-DC converter design is presented using MATLAB simulation.

6. **Chapter 6** provides a summary of the major findings, contributions, and suggestions for future research directions. This chapter serves as a conclusion, encapsulating the key outcomes of the study and highlighting its significance. Additionally, it points towards potential avenues for further exploration and investigation in related areas.

CHAPTER 2

LITERATURE REVIEW

2.1 Literature Review

Solar photovoltaic (PV) technology offers versatility, enabling electricity generation across a wide range of applications. While the high initial investment has traditionally been a significant drawback, advancements in mass production have substantially reduced costs in recent years, with further cost reductions expected in the future. Compared to fuel cell based generation it is still lower. The rapid expansion of power electronic technology underscores its importance in successfully integrating renewable energy generation into the power grid, as highlighted in references [10-12]. For the stepping up of low voltage generated from PV it is important to incorporate power electronic converter which showcases high gain. This implementation aims to ensure the preservation or enhancement of power supply quality and reliability. The converter serves as a vital component, facilitating the integration of PV with the high voltage bus, while prioritizing the consistent delivery of reliable power. Isolated converters with high frequency transformer (HF) are preferred over non-isolated topologies due to their advantages such as high step-up ratio, galvanic isolation, and flexible system setup [13-18]. There are options available for both current-fed and voltage-fed HF transformer isolated converters [19-21] and [22-32]. A comparison of the benefits and drawbacks of both types is presented in [33–35]. Low switch voltage rating being the advantage of voltage fed converters enable them to use low power rating switches but these converters suffers from may disadvantages like large pulsating current at input, lower efficiency for high voltage step up applications, presence of circulating current in higher magnitude, low range soft switching, loss of duty cycle in case of inductive output filter. As compared to voltage fed converter current fed converter comes up with advantages like lower ripples at input, smaller size transformer , no ringing in rectifier diodes, loss of duty cycle is mitigated , easier control and can be used for high current applications. They are particularly well-suited for integrating the low-voltage, high-current outputs from renewable energy sources such as solar photovoltaic (PV) systems and fuel cells with high-voltage DC buses. Among the isolated current-fed DC-DC converter topologies, three have been

extensively studied: full-bridge [36–38], L-type half bridge [39–41], and push-pull [42–43]. In medium or high power applications requiring isolated step-up DC-DC conversion, the most common choices are the half-bridge, full-bridge (FB), and push-pull (PP) architectures. When a high-voltage conversion ratio is needed, a half-bridge converter typically requires twice the turn ratio compared to full-bridge converters. This leads to increased primary current rating and high-frequency (HF) transformer leakage inductance. Consequently, PP or FB converters are preferred in such scenarios. The PP converter offers advantages over the FB converter, such as a reduced number of power switches and lower conduction losses, making it well-suited for low-voltage, high-current step-up applications [44–47].However, it is important to note that traditional current-fed and voltage push-pull converters exhibit hard switching due to transformer leakage inductance, resulting in switching losses and high turn-off voltage spikes. To address these challenges and achieve soft switching, numerous enhanced topologies have been proposed in the literature. These include ZVS [48–50], ZCS [51], voltage spike clamping and suppression [52]. Active-clamp circuits [53], RCD passive snubbers [54], and energy-recovery snubbers [55]. RCD snubbers, although simple, have lower efficiency as the energy absorbed by the clamping capacitor is dissipated in the resistor. Under light loads, the active clamp in the converter encounters challenges such as high current stress (peak) and increased circulating current. In an effort to achieve zero-voltage switching (ZVS) for the switches, an active-clamp-based ZVS topology was proposed, analyzed, and developed in [56]. However, this topology has drawbacks, including consuming approximately 2% of the output power, increasing conduction losses due to the higher circulating current, and adding complexity and component count to the converter. To improve power conversion efficiency and reduce switching losses, research has been conducted on zero-current switching (ZCS) and ZVS soft-switching technology for the PP converter over the years. Current-fed PP converters can achieve ZCS by utilizing the built-in commutation modes of the converter without the need for additional hardware. PP converters proposed in [57] and [58] uses an active switch on the primary side of the HF centre tapped transformer, which results in ZVS turn-on of the primary switches. Although these converter cannot achieve ZVS under light load condition. Other approaches, such as designing the magnetizing inductor of the converter in [59] and [60] to provide ZVS performance across a wide load range, have been explored. For improving the efficacy of PP topologies resonant tank circuits such

as LC, LLC and LCL [61] are used either on the primary or the secondary side. Extra capacitors are required with the leakage inductance of the HF transformer to extend the soft switching range of the converter and achieve ZCS and ZVS. There are other solutions also such as usage of auxiliary circuits like buck or flyback circuits to control the gain of the output voltage. Although these configurations enable step-down and step-up functions, they introduce additional components and complexity. In [62], all active switches are capable of achieving zero-voltage switching (ZVS) and are positioned on both the main and secondary sides. However, this approach requires expensive and complex driving circuits. References [63] and [64] experience drawbacks such as duty cycle loss and reduced voltage gain of the converter, respectively. Additionally, there are secondary rectifier diodes that exhibit high-voltage ringing. In [65] and [66], two active clamping circuits are added to the primary side to recycle leakage energy, enabling ZVS implementation. However, the auxiliary switches in these cases are subjected to voltage stresses that exceed twice the input voltage. In [67] a buck-boost circuit is used for active clamping where all the power switches can achieve ZVS when two active auxiliary switches are included. Although the limitation of this the need of intricate drivers for additional power switches was present. To address the issues mentioned, a clamping capacitor is introduced between the switches in the proposed push-pull architecture [68]. Transformer leakage inductors are utilized to eliminate the effects of leakage inductance and facilitate energy transfer buffering. However, the main switches still operate under hard switching conditions. In response to this problem, a topology was previously proposed in [69], which adds an auxiliary switch at the input end to achieve soft switching over a wide range of loads. However, this approach requires the energy stored in the output end filter inductor, and the diode fails to achieve soft turn-off. Moreover, there are challenges associated with high-voltage stress across the switch and secondary rectifier voltage ringing.

2.2 Conclusion

From the above literature review it can be concluded that a highly efficient, less costly current fed push pull converter with simple circuitry, lesser power switches, no auxiliary circuit for clamping at the primary side, soft switching technique for increasing efficiency, ground referred switches with single gate driver requirement and easier control is needed for the integration of PV with the grid.

CHAPTER 3

CONVENTIONAL CURRENT FED PUSH PULL CONVERTER

3.1 Introduction

A current-fed converter is a device that switches current rather than voltage to function. Fig. 3.1 represents the circuit of current fed push pull converter. The current-fed push-pull converter differs from the voltage-fed push-pull converter by shifting the inductor L_{IN} from the output side to the input side of the transformer. One of the main advantages of the current-fed push-pull converter is its inherent short-circuit protection. The converter is less vulnerable to short-circuit damage because the input current source delivers consistent current. Owing to this feature, it is appropriate for applications where dependability and robustness are essential, including industrial power systems. Additionally, the current-fed push-pull converter provides good output voltage and current control. By adjusting the duty cycle of the switches, it becomes possible to achieve accurate output regulation. Applications that require reliable and adaptable power sources, such as renewable energy systems, electric vehicles, and telecommunication equipment, can benefit from this level of control. When it comes to efficiency, the current-fed push-pull converter surpasses voltage-fed converters. Since the input source is a current source, power can be delivered to the load directly without the need for a resistor in series to limit the current. As a result, it becomes a more appealing option for high-power applications and lowers power losses overall .In comparison to its voltage-fed equivalents, the current-fed push-pull converter also exhibits less EMI. The primary transformer winding aids in isolating the input source from the output, minimizing EMI, and reducing the spread of noise. This characteristic is especially useful in delicate applications, such as medical equipment and communication systems.

3.2 System Configuration

The conventional current fed push pull converter configuration employs two switches at the primary side with an input inductor as shown Fig. 3.1.The current is sent through winding P_1 by switch S_1, and through winding P_2 by switch S_2. The current splits equally between the windings when both switches are closed. A current path can only be created by closing at least one switch. Fig. 3.2 displays the waveforms and

switching order. The converter operates on low voltage DC bus having voltage of 48 V. The converter is designed for 500W application. The fast recovery SiC diodes on the output side of the HF transformer are expected to produce a DC bus with an output voltage of 380V and a capacitive filter is employed at the output side that filters voltage ripple of the output voltage.

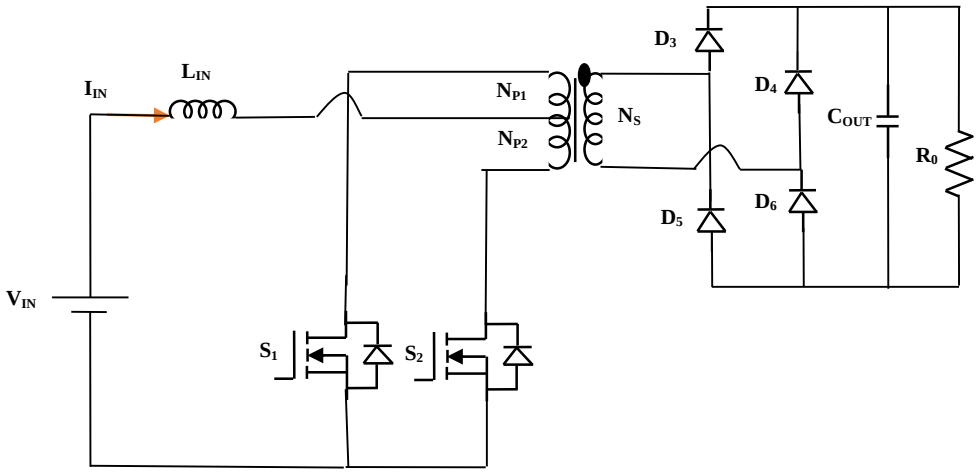

Fig. 3.1 Schematic of Proposed Converter

3.3 Modes of Operation and Mathematical Modelling

In this section, the steady-state operation and analysis of the conventional current-fed push-pull converter are summarized. The associated mathematical equations and assumptions are also presented. The waveforms under steady state conditions are shown in Fig. 3.2. Analytical equations that were created can be used to evaluate component quantities and ratings as well as the theoretical converter performance.

The following presumptions are introduced in order simplify theoretical analysis:

1) The capacitance of the output capacitor C_{OUT} is sufficiently large, allowing the steady-state analysis to disregard output voltage ripple.

2) The duration of the commutation interval is very brief, resulting in negligible changes in both the transformer's magnetizing current and the input inductor current.

3) The transformer operates symmetrically without bias magnetization.

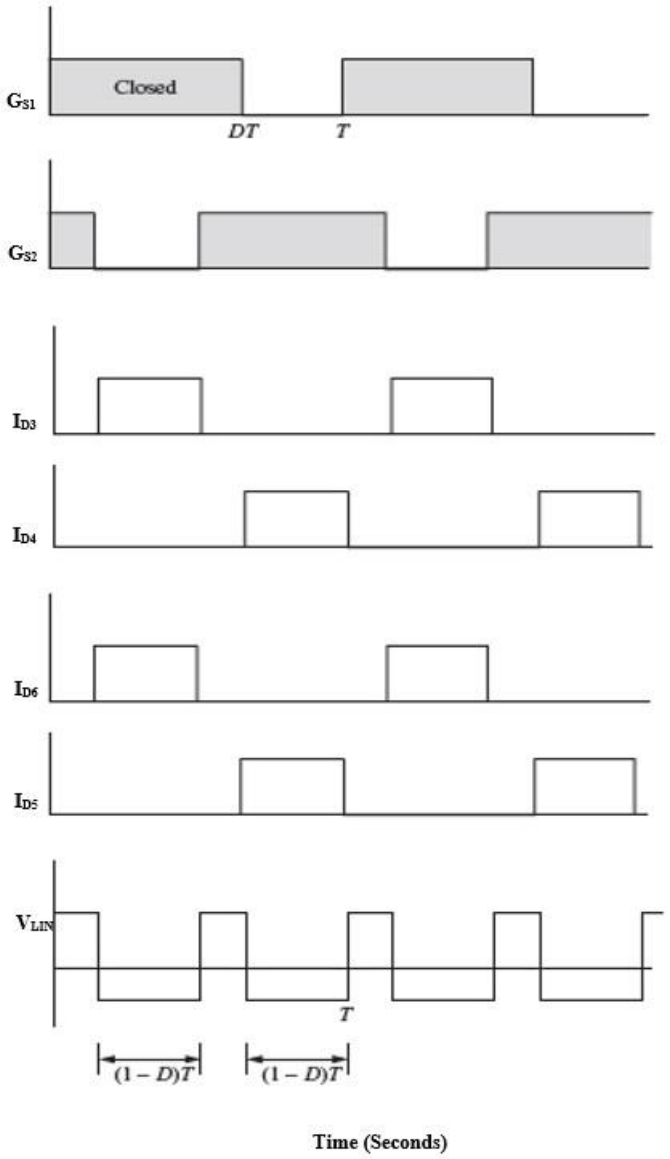

Fig. 3.2 Switching pulses and steady state waveforms

A. S_1 Closed and S_2 Open

When switch 1 is closed and switch 2 is open, the input current I_{IN} passes through the primary winding P_1 as well as through D_3 and D_6 on the secondary side. At this stage, D_3 and D_6 are in an active state, while D_4 and D_5 are inactive. The following equations are applicable in this scenario:

$$i_{D_3} = I_{IN} \frac{N_P}{N_S} \tag{3.1}$$

$$V_{P_1} = V_o \frac{N_P}{N_s} \tag{3.2}$$

$$V_{L_{IN}} = V_{IN} - V_{P_1} = V_{IN} - V_O \left(\frac{N_P}{N_s}\right) \tag{3.3}$$

$$V_{S_2} = V_{P_1} + V_{P_2} = 2V_o \left(\frac{N_P}{N_S}\right) \tag{3.4}$$

B. S_1 Open and S_2 Closed

When switch 1 is open and switch 2 is closed, the input current I_{IN} passes through primary winding P_2 and flows through D_2 on the secondary side. At this state, D_3 and D_6 are inactive, while D_4 and D_5 are active. The following equations are applicable in this situation:

$$i_{D_4} = I_{IN} \left(\frac{N_P}{N_S}\right) \tag{3.5}$$

$$V_{P_2} = V_o \left(\frac{N_P}{N_S}\right) \tag{3.6}$$

$$V_{L_{IN}} = V_{IN} - V_o \left(\frac{N_P}{N_S}\right) \tag{3.7}$$

$$V_{S_1} = V_{P_1} + V_{P_2} = 2V_O \left(\frac{N_P}{N_S}\right) \tag{3.8}$$

C. Both S_1 and S_2 Closed

When both switches are closed, the input current I_{IN} is evenly distributed between the two primary windings, and all diodes are in an inactive state. The voltage across each primary winding is zero:

$$V_{P_1} = V_{P_2} = 0 \tag{3.9}$$

Inductor L_{IN} then has the source voltage across it:

$$V_{L_{IN}} = V_{IN} \tag{3.10}$$

To maintain steady-state operation, the average voltage across L_{IN} must be zero. Within one switching period, the voltage across L_{IN} can be expressed as follows: $V_{L_{IN}} = V_{IN} - V_o\left(\frac{N_P}{N_s}\right)$ during the two intervals of $(1-D)T$ when only one switch is closed, and $V_{L_{IN}} = V_{IN}$ during the remaining time, which is $T - 2(1-D)T = (2D-1)T$. Hence, the average inductor voltage can be calculated as:

$$V_{L_{IN}} = V_{IN}(2D-1)T + \left[V_{IN} - V_o\left(\frac{N_P}{N_s}\right)2(1-D)T\right] = 0 \tag{3.11}$$

Solving for V_o,

$$V_o = \frac{V_{IN}}{2(1-D)}\left(\frac{N_S}{N_P}\right) \tag{3.12}$$

Where D is the duty ratio of each switch. This result is similar to that of the boost converter.

TABLE I SIMULATION PARAMETERS

Parameter	**Values**
Input voltage	48 V
Output voltage	380 V
Output power	500 W
Switching frequency	100 kHz
Turns Ratio	1:1:7.9
Leakage inductance ($LLeakage1$and $LLeakage2$ **)**	2 μH
Inductance of boost inductor	500 μH
Output capacitor	220 μF

3.4 Simulation Results

To validate the theoretical analysis, the circuit of the conventional current fed push pull converter is constructed in MATLAB Simulink. The converter is tested with a 48 V DC input voltage with a 100 kHz switching frequency. The output voltage and power requirements are 380V and 500W, respectively. At the specified input voltage, the

Duty D is calculated to be 0.50. The transformer T's leakage inductances, $L_{Leakage1}$ and $L_{Leakage2}$, are both equal to 2µH. The maximum ripple in input current $I_{IN\,ripple}$, max is set to 0.2 A by employing an input inductor L_{IN} of 500µH. Table I contains the list of crucial simulation parameters.

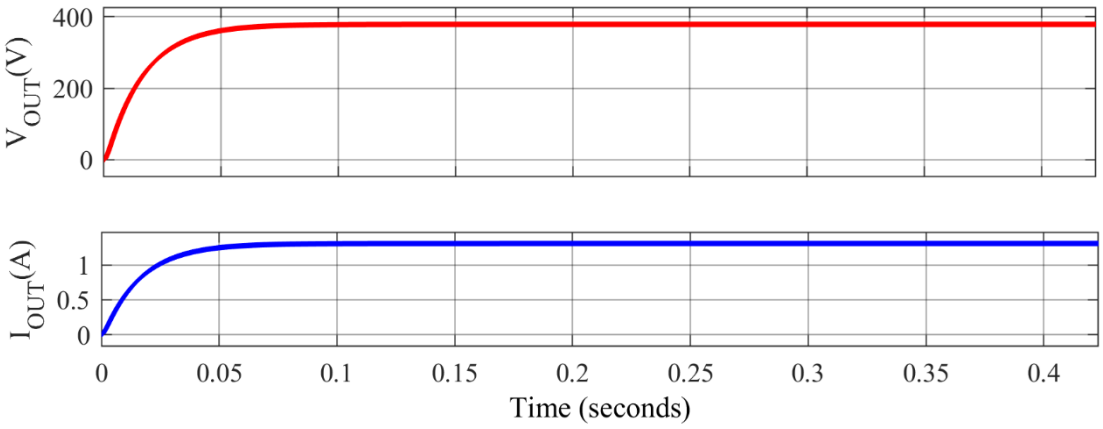

Fig. 3.3 Output Voltage $V_{OUT}(V)$ and Output Current $I_{OUT}(A)$

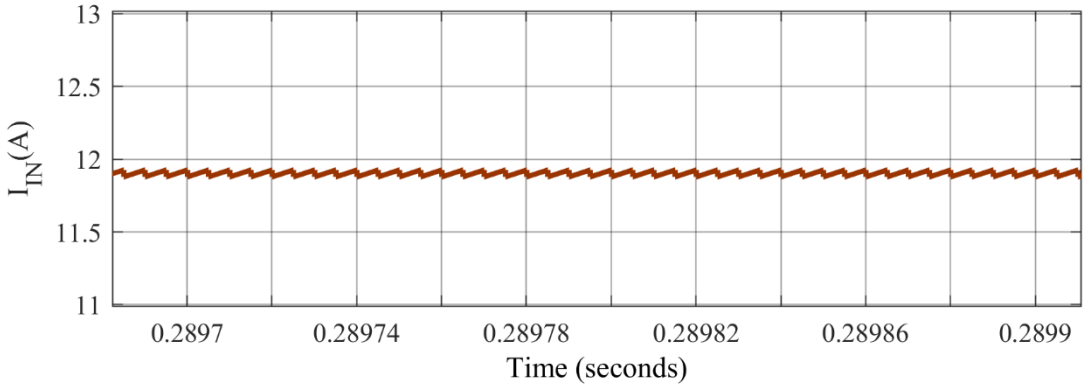

Fig. 3.4 Input Current $I_{IN}(A)$

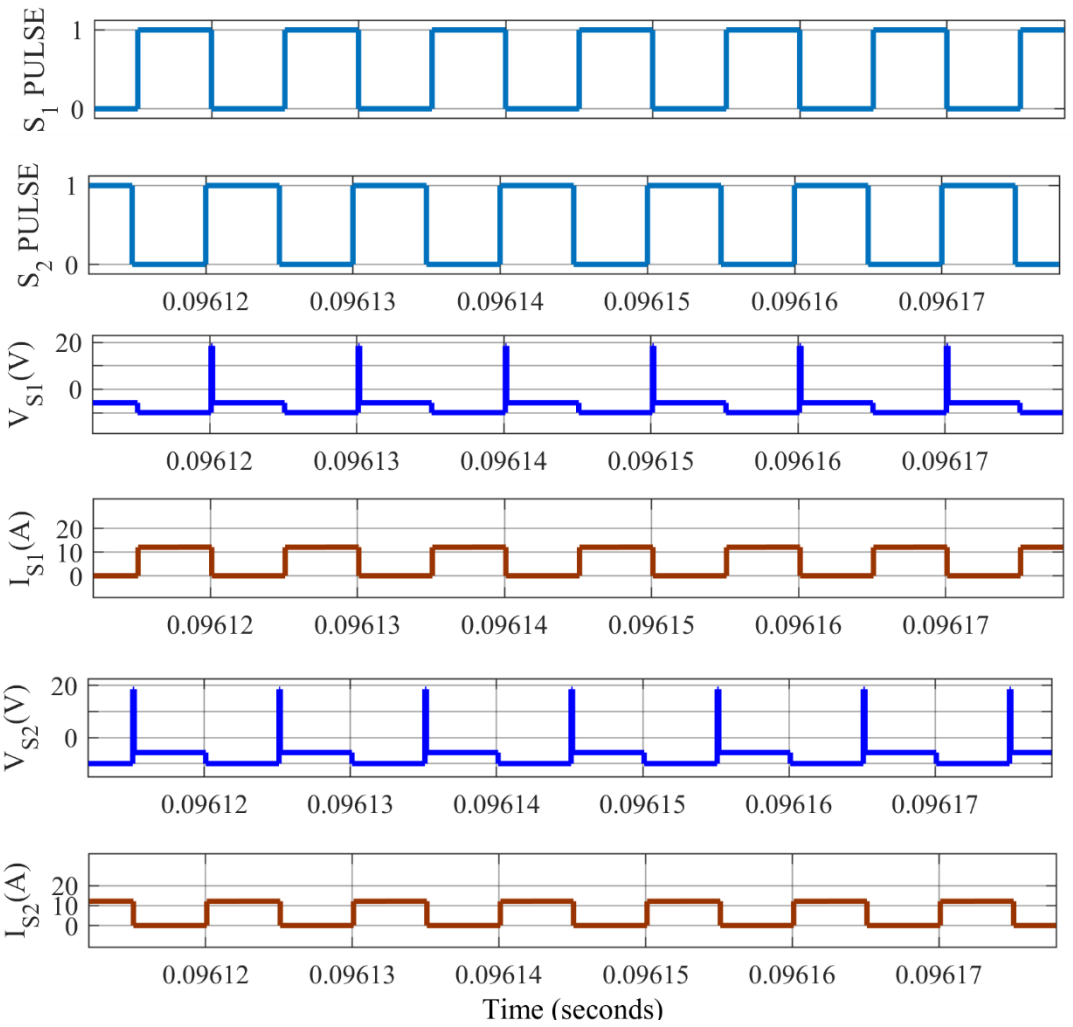

Fig. 3.5 S_1 and S_2 gate pulses with drain to source voltage and current

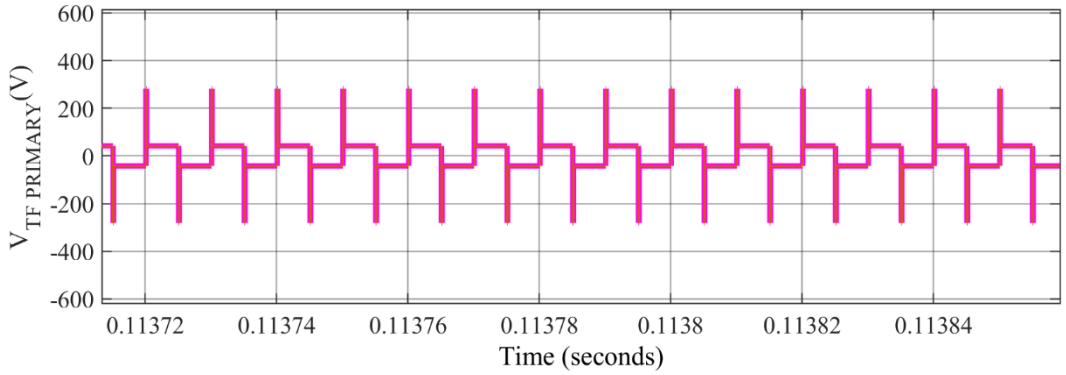

Fig. 3.6 Transformer primary voltages $V_{TF\ PRIMARY}(V)$

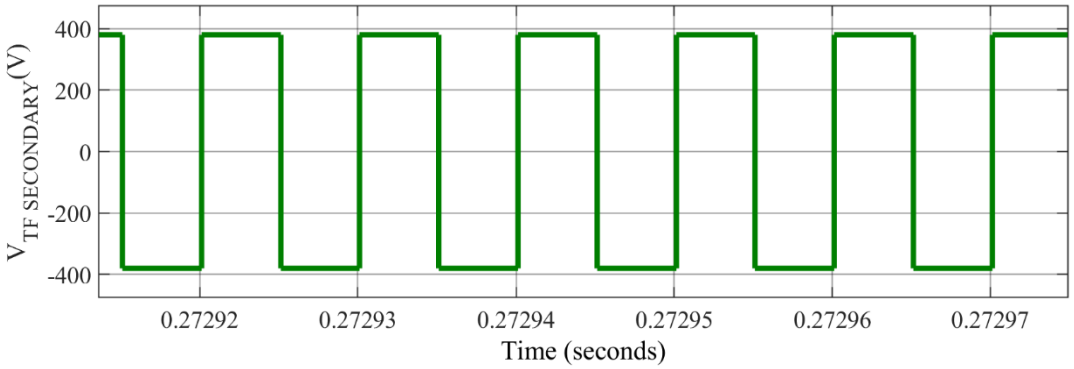

Fig. 3.7 Transformer secondary voltage $V_{TF\ SECONDARY}(V)$

Fig. 3.3 shows the output current and voltage waveforms. Because there is no overshoot or undershoot in the output waveforms, the settling time is reduced, and the required rating of the output capacitor is decreased. Due to the inductor's (L_{IN}) presence at the input, the maximum ripple current seen in Fig. 3.4 input current waveform is restricted to 0.2A. Fig. 3.5 displays the waveforms of the current and drain to source voltages for switches S_1 and S_2, in addition to the gating signals for each switch. As illustrated in Fig. 3.5, high voltage spike can be seen across switches S_1 and S_2 when the switches turns off. This increases the conduction losses in the switches and decreases efficiency. Fig. 3.6, respectively, shows the waveforms of the primary voltage of the HF transformer and it can be seen that high voltage spike is present due to which there is a chance of insulation breakdown and if the high voltage spike exceeds transformer's saturation limit the magnetic core can become saturated this leads to increase in core losses and reduction in efficiency. As a result of the inclusion of quick recovery SiC diodes on the output side, the problem of reverse recovery is minimized. Transformer's secondary voltage waveform is shown in Fig 3.7.

CHAPTER 4
DUAL CAPACITOR TRAPPED ZCS PUSH PULL CURRENT FED CONVERTER FOR RENEWABLE ENERGY CONVERSION SYSTEM

4.1 Introduction

A dual capacitor trapped current fed ZCS push-pull converter has been analyzed and designed for renewable energy conversion applications in this chapter. Owing to the resonance between the trapped capacitors and the leakage inductances of the HF transformer, the topology maintains ZCS on the trailing edges and inherent voltage suppression at leading edges. The effective mitigation of voltage spikes across power devices allows for the utilization of low voltage, low power devices. There is no overshoot or undershoot in the output current and voltage consequently, the settling time is reduced, and the required rating of the output capacitor decreases. In the proposed converter, no auxiliary circuit is involved, and because all switches are ground referred, a non-isolated driver with a single power supply can be employed. A comprehensive study of a scaled down model of 500W and the design of the proposed converter, including mathematical analysis, has been presented in this chapter.

4.2 System Configuration

The proposed converter configuration employs a dual capacitor trapped ZCS operation of the 500W current fed push pull converter as shown in Fig. 4.1. The converter operates on low voltage DC bus having voltage of 48V. On the primary side of a traditional push-pull converter, the new architecture uses two identical trapped capacitors with series diodes in order to accomplish ZCS operation of the switches. The fast recovery SiC diodes on the output side of the HF transformer are expected to produce a DC bus with an output voltage of 380V and a capacitive filter is employed that filters voltage ripple on the output side.

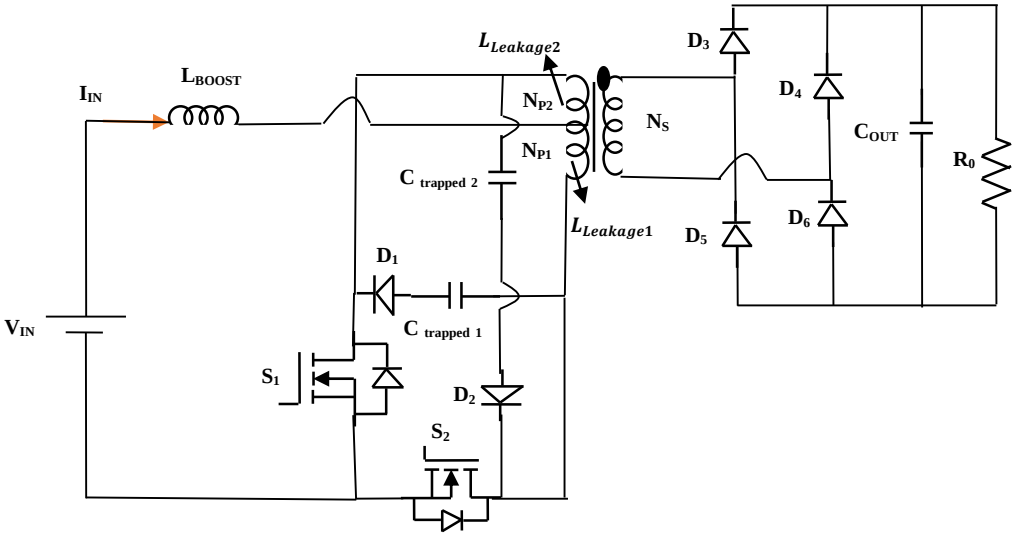

Fig. 4.1 Schematic of Proposed Converter

4.3 Modes of Operation

In this section, the steady-state operation and analysis of the proposed dual capacitor trapped ZCS push-pull converter are summarized. The associated mathematical equations and assumptions are also presented. The transformer leakage inductance $L_{leakage}$ and a dual trapped capacitors $C_{trapped\ 1}$ and $C_{trapped\ 2}$ make up the resonant tank for the ZCS operation of the primary switches. The switches gating signals are 180 °phase-shifted and have a duty cycle D that is greater than 50%. After the first half cycle's analysis was finished, the intervals for the second half cycle were repeated with the other symmetrical devices conducting. Analogous circuits that depict the converter's working modes are shown in Fig. 4.3.

Analytical equations that were created can be used to evaluate component quantities and ratings as well as the theoretical converter performance.

The following presumptions are introduced in order simplify theoretical treatment.

1) The circuit operation is in a steady state.
2) The capacitance of the output capacitor C_{OUT} is sufficiently large, allowing the steady-state analysis to disregard output voltage ripple.
3) The duration of the commutation interval is very brief, resulting in negligible changes in both the transformer's magnetizing current and the input inductor

current.

4) The windings in the transformer T are tightly coupled with one another, and have negligibly small resistance.

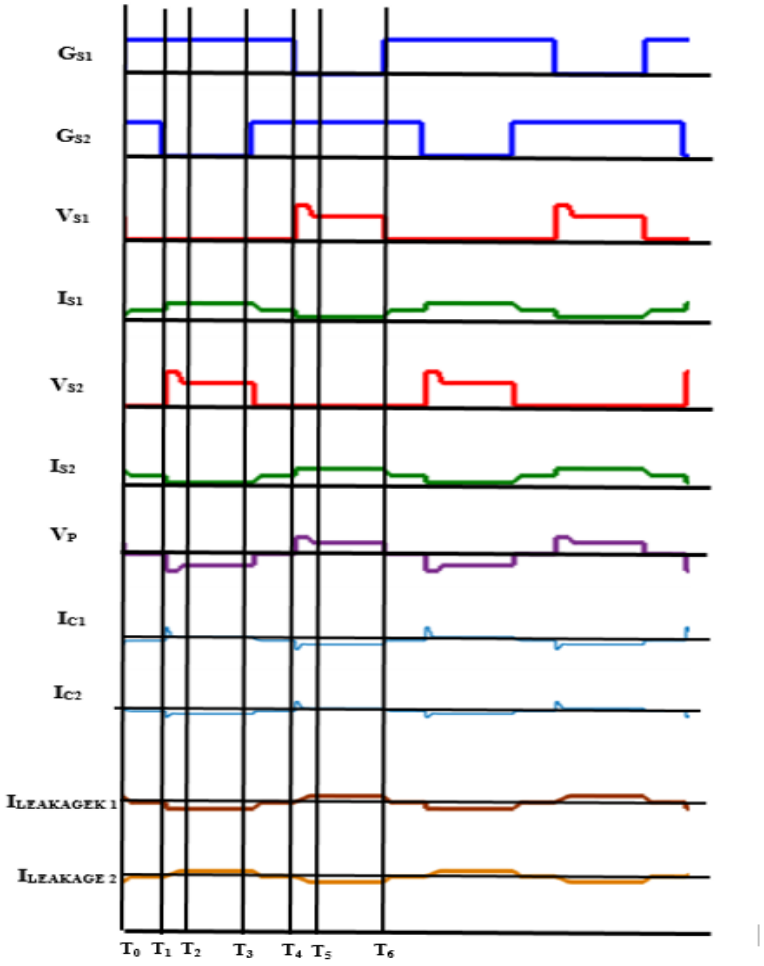

Fig. 4.2 Switching pulses and steady state waveforms

A. Interval 1((Fig. 4.2 : $T_0 < t < T_1$) Mode 3(Fig. 4.3(c)) :

In this short interval the switch S_1 gets just turn ON and the capacitors C_2 starts discharging and C_1 starts charging until the current through both switches becomes equal and HF transformers Leakage inductors charge is transferred to the trapped capacitor resulting in ZCS turn ON operation of the switch S_1. The current through $L_{Leakage1}$ starts decreasing and $L_{Leakage2}$ starts increasing until the current across both switches becomes equal in magnitude.

B. Interval 2 ((Fig. 4.2 : $T_1 < t < T_2$) Mode 1(Fig. 4.3(a)) :

In this interval the primary side switch S_1 is already conducting and switch S_2 just turns OFF and diode D_4 and D_5 of secondary side rectifier bridge are conducting. The current through the $I_{Leakage1}$ decreases and $I_{Leakage2}$ increases until the capacitor C_1 charges and C_2 discharges to achieve voltage clamping on the leading edges of the switch S_2.

C. Interval 3 ((Fig. 4.2 : $T_2 < t < T_3$) Mode 1(Fig. 4.3(a)) :

In this interval the primary side switch S_1 is already conducting and switch S_2 is OFF and diode D_4 and D_5 of secondary side rectifier bridge are conducting. Constant current I_{IN} flows through $L_{Leakage2}$ .Switch S_1 carries the entire input current.

D. Interval 4 ((Fig. 4.2 : $T_3 < t < T_4$) Mode 3(Fig. 4.3(c)) :

In this interval the switch S_2 gets just turn ON and the capacitors C_1 starts discharging and C_2 starts charging until the current through both switches becomes equal and HF transformers Leakage inductors charge is transferred to the trapped capacitor resulting in ZCS turn ON operation of the switch S_2. The current through $L_{Leakage2}$ starts decreasing and $L_{Leakage1}$ starts increasing until the current across both switches becomes equal in magnitude.

E. Interval 5 ((Fig. 4.2 : $T_4 < t < T_5$) Mode 2(Fig. 4.3(b)) :

In this interval the primary side switch S_2 is already conducting and switch S_1 turns OFF and diode D_3 and D_6 of secondary side rectifier bridge are conducting. The current through the $I_{Leakage1}$ increases and $I_{Leakage2}$ decreases until the capacitor C_2 charges and C_1 discharges to achieve voltage clamping on the leading edges of the switch S_1.

F. Interval 5 ((Fig. 4.2 : T_5 <t< T_6) Mode 2(Fig. 4.3(b)) :

In this interval the primary side switch S_2 is already conducting and switch S_1 is OFF and diode D_3 and D_6 of secondary side rectifier bridge are conducting. Constant current I_{IN} flows through $L_{Leakage1}$ .Switch S_2 carries the entire input current.

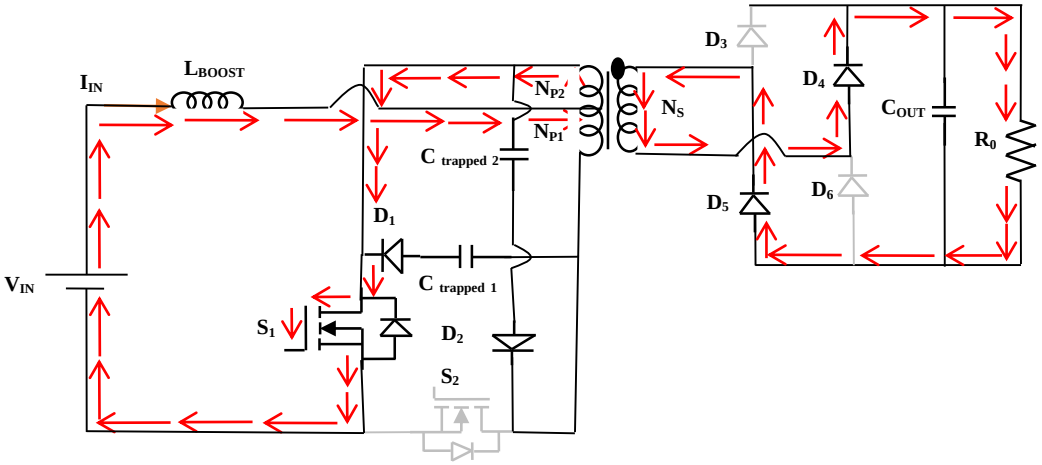

Fig. 4.3(a) Modes of Operations (Mode 1)

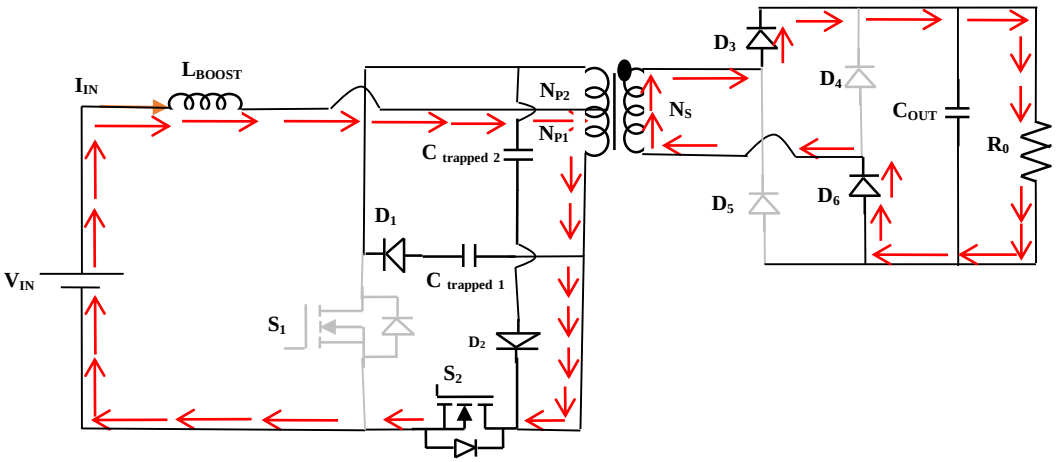

Fig. 4.3(b) Modes of Operations (Mode 2)

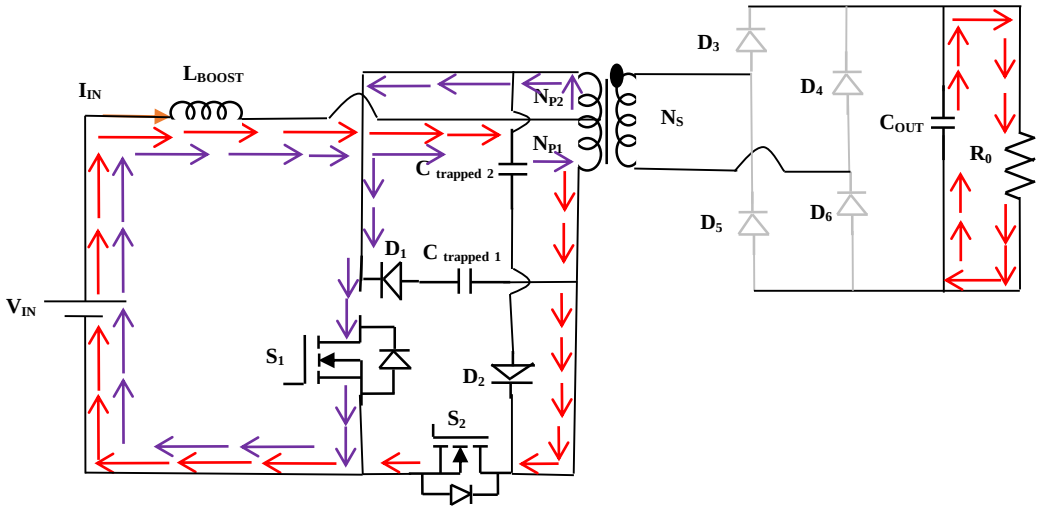

Fig. 4.3(c) Modes of Operations (Mode 3)

4.4 Mathematical Analysis

The study of the dual trapped capacitor current fed push-pull converter depicted in Fig. 4.1 is explained in this section. High efficiency, ZCS, and a low switching surge are some of this converter's distinguishing features. Furthermore, the series connection of the inductor with the input power source provides a high level of immunity against external noise and effectively suppresses backward noise. In this study, three operating modes are examined: the first when only switch S_2 is conducting, and the second when both switches S_1 and S_2 are conducting and third when only switch S_1 is conducting. Second, an in-depth assessment of the effects of the trapped capacitors and leakage inductance of the transformer was made. The first step in the analytical procedure is the derivation of differential equations that capture the low-frequency behavior of the resonant converter. In this analysis, differential equations are developed and a few analytical expressions are clarified. There is further discussion of the calculations for the static and dynamic properties. Our mathematical model takes into account trapped capacitors and the transformer's inductance. Parasite resistances were not taken into consideration. Diodes are regarded as ideal for the analysis.

$V_{IN(t)}$: Input Voltage
$V_{DS1}(t), V_{DS2}(t)$: Drain to Source Voltage of Mosfet Switch S_1 and S_2 respectively
$V_{C1trapped}(t)$: Voltage across trapped capacitor $C_{trapped\ 1}$
$V_{C2trapped}(t)$: Voltage across trapped capacitor $C_{trapped\ 2}$
$I_{C1trapped}(t)$: Current through trapped capacitor $C_{trapped\ 1}$
$I_{C2trapped}(t)$: Current through trapped capacitor $C_{trapped\ 2}$

$I_{IN\ BOOST}(t)$: Input inductor current
$I_{OUT}(t)$: Output current
$V_{OUT}(t)$: Output Voltage
$L_{LT}(t)$: Total leakage inductance of transformer's primary

A. State 1: When S2 is ON

The circuit equations in this interval are:

$$V_{IN} = L_{Boost}\frac{di}{dt} + \frac{d\emptyset}{dt} \tag{4.1}$$

Here, ∅ represents the linkage flux associated with the primary winding of the transformer.

$$I_{C2\ trapped} = C_{2trapped}\frac{dV_{C2\ trapped}}{dt} \tag{4.2}$$

$$(I_{IN} - I_{C2\ trapped}) - I_{C2\ trapped} - nI_{OUT} = \frac{\emptyset}{L_{TF}} \tag{4.3}$$

$$V_{C2\ trapped} = 2\frac{d\emptyset}{dt} \tag{4.4}$$

$$C_{OUT}\frac{dV_{OUT}}{dt} + \frac{V_{OUT}}{R} = I_{OUT} \tag{4.5}$$

Where n is turns ratio of transformer

$$n = \frac{N_2}{N_1} \tag{4.6}$$

Equation (4.3) represents the relation of transformers magnetizing current and linkage flux. By using Laplace transform technique to solve equation (4.1) to (4.5) we get

$$\emptyset(t) = \emptyset(0) + A\left(t - \frac{\sin w_0 t}{w_0}\right) + \frac{B}{w_0}(1 - \cos w_0 t) \tag{4.7}$$

$$I_{IN}(t) = I_{IN}(0) + \frac{V_{IN}(t)}{L} - \frac{A}{L}\left(t - \frac{\sin w_0 t}{w_0}\right) - \frac{B}{w_0 L}(1 - \cos w_0 t) \tag{4.8}$$

$$V_{OUT}(t) = V_{OUT}(0)\left(1 - \frac{t}{C_{OUT}R} - \frac{t^2}{2C_{OUT}}\right) + \frac{I_{OUT}(0)t}{C_{OUT}} - \frac{nAC_{OUT}R^2}{1 + (w_0 C_{OUT}R)^2}\left[1 - \frac{t}{C_{OUT}R} - \frac{{w_0}^2 t^2}{2} - \cos w_0 t + \frac{\sin w_0 t}{w_0 C_{OUT}R}\right] + \frac{nBC_{OUT}R^2}{1 + (w_0 C_{OUT}R)^2}\left[\frac{1}{w_0 C_{OUT}R} + w_0 t - \frac{\cos w_0 t}{w_0 C_{OUT}R} - \sin w_0 t\right] \tag{4.9}$$

$$V_{C2\ trapped}(t) = 2A(1 - \cos w_0 t) + 2B \sin w_0 t \tag{4.10}$$

Where $\emptyset(0)$, $I_{IN}(0)$,$V_{OUT}(0)$, $I_{OUT}(0)$are initial values in this interval and the resonance frequency w_o and parameters A and B are:

$$w_0 = \frac{1}{2}\sqrt{\frac{1}{C_{2trapped}}\left(\frac{1}{L_{TF}}\right)} \tag{4.11}$$

$$A = \frac{V_{IN} + nV_{OUT}L}{4{w_0}^2 L C_{2trapped}} \tag{4.12}$$

$$B = \frac{I_{IN}(0) - nI_{OUT}(0) - \frac{\emptyset(0)}{L_{TF}}}{4w_0 C_{2trapped}} \tag{4.13}$$

The transition to the next state occurs when the resonance voltage $V_{C2\ trapped}$ reaches zero.

B. State 2: When S1 and S2 both on

From the above equivalent circuit we get:

$$V_{IN} = L_{BOOST}\frac{di}{dt} \tag{4.14}$$

$$C_{OUT}\frac{dV_{OUT}}{dt}+\frac{V_{OUT}}{R}=0 \tag{4.15}$$

Using Laplace transform,

$$\emptyset(t)=\emptyset(t1) \tag{4.16}$$

$$I_{IN}(t)=\frac{V_{IN}}{L}(t-t_1) \tag{4.17}$$

$$V_{OUT}(t)=V_{OUT}(t1)\left(1-\frac{t-t_1}{C_{OUT}R}\right) \tag{4.18}$$

Where t_1 is the time when both switches S_1 and S_2 are ON.

C. State 3: When S1 is ON

The circuit equations in this interval are:

$$V_{IN}=L_{Boost}\frac{di}{dt}+\frac{d\emptyset}{dt} \tag{4.19}$$

Where $\emptyset$ is linkage flux associated with primary winding of the transformer.

$$I_{C1\,trapped}=C_{1trapped}\frac{dV_{C1\,trapped}}{dt} \tag{4.20}$$

$$(I_{IN}-I_{C1\,trapped})-I_{C1\,trapped}-nI_{OUT}=\frac{\emptyset}{L_{TF}} \tag{4.21}$$

$$V_{C1\,trapped}=2\frac{d\emptyset}{dt} \tag{4.22}$$

Where n is turns ratio of transformer

$$n=\frac{N_2}{N_1} \tag{4.23}$$

Equation (4.21) represents the relation of transformers magnetizing current and linkage flux. By using Laplace transform technique to solve equation (4.19) to (4.23) we get

$$\emptyset(t) = \emptyset(0) + A\left(t - \frac{\sin w_0 t}{w_0}\right) + \frac{B}{w_0}(1 - \cos w_0 t) \tag{4.24}$$

$$I_{IN}(t) = I_{IN}(0) + \frac{V_{IN}(t)}{L} - \frac{A}{L}\left(t - \frac{\sin w_0 t}{w_0}\right) - \frac{B}{w_0 L}(1 - \cos w_0 t) \tag{4.25}$$

$$\begin{aligned} V_{OUT}(t) = V_{OUT}(0)\left(1 - \frac{t}{C_{OUT}R} - \frac{t^2}{2C_{OUT}}\right) + \frac{I_{OUT}(0)t}{C_{OUT}} \\ - \frac{nAC_{OUT}R^2}{1 + (w_0 C_{OUT}R)^2}\left[1 - \frac{t}{C_{OUT}R} - \frac{{w_0}^2 t^2}{2}\right. \\ \left. - \cos w_0 t + \frac{\sin w_0 t}{w_0 C_{OUT}R}\right] \\ + \frac{nBC_{OUT}R^2}{1 + (w_0 C_{OUT}R)^2}\left[\frac{1}{w_0 C_{OUT}R} + w_0 t\right. \\ \left. - \frac{\cos w_0 t}{w_0 C_{OUT}R} - \sin w_0 t\right] \end{aligned} \tag{4.26}$$

$$V_{C1\,trapped}(t) = 2A(1 - \cos w_0 t) + 2B \sin w_0 t \tag{4.27}$$

Where $\emptyset(0)$, $I_{IN}(0)$,$V_{OUT}(0)$, $I_{OUT}(0)$are initial values in this interval and the resonance frequency w_o and parameters A and B are :

$$w_0 = \frac{1}{2}\sqrt{\frac{1}{C_{1trapped}}\left(\frac{1}{L_{TF}}\right)} \tag{4.28}$$

$$A = \frac{V_{IN} + nV_{OUT}L}{4{w_0}^2 L C_{1trapped}} \tag{4.29}$$

$$B = \frac{I_{IN}(0) - nI_{OUT}(0) - \frac{\emptyset(0)}{L_{TF}}}{4w_0 C_{1trapped}} \tag{4.30}$$

Putting the differentiation in the above differential equations and to be zero static characteristics are derived.

$$2\emptyset = A\left(t - \frac{\sin w_0 t}{w_0}\right) + \frac{B}{w_0}(1 - \cos w_0 t) \tag{4.31}$$

$$V_{IN}T_S = A\left(t - \frac{\sin w_0 t}{w_0}\right) + \frac{B}{w_0}(1 - \cos w_0 t) \tag{4.32}$$

$$V_{OUT}T_S = nA\left(t - \frac{\sin w_0 t}{w_0}\right) + \frac{nB}{w_0}(1 - \cos w_0 t) \quad (4.33)$$

Where $\emptyset$ is linkage flux and T_S is the switching period of the converter operation.

Above equations yields the following results

$$|\emptyset| = \frac{1}{2}V_{IN}T_S \quad (4.34)$$

$$V_{OUT} = nV_{IN} \quad (4.35)$$

Maximum value $V_{C1\ trapped\ \max}$ and $V_{C2\ trapped\ \max}$ of the resonance voltage is derived from the equation (4.) as follows:

$$V_{C1\ trapped\ ,max} = V_{C2\ trapped\ ,max} = 2A + 2\sqrt{A^2 + B^2} \quad (4.36)$$

TABLE II SIMULATION PARAMETERS

Parameter	**Values**
Input voltage	48 V
Output voltage	380 V
Output power	500 W
Switching frequency	100 kHz
Turns Ratio	1:1:4.3
Leakage inductance ($L_{Leakage1}$and $L_{Leakage2}$ **)**	2 μH
Inductance of boost inductor	500 μH
Trapped capacitor ($C_{trapped1}$ and $C_{trapped2}$)	100 nF
Output capacitor	220 μF

4.5 Simulation Results

To validate the theoretical analysis, the circuit of the proposed dual capacitor trapped ZCS push pull converter is constructed in MATLAB Simulink. The converter is tested with a 48V DC input voltage with a 100 kHz switching frequency. The output voltage and power requirements are 380V and 500W, respectively. At the specified input voltage, the Duty D is calculated to be 0.65. The transformer T's leakage inductances, $L_{Leakage1}$ and $L_{Leakage2}$, are both equal to 2µH. The maximum ripple current I_{IN}, max is set to 0.5A at D 0.65 by employing a boost inductor L_{BOOST} of 500µH. To accomplish ZCS, two trapped capacitors ($C_{trapped\,1}$ and$C_{trapped\,2}$) with a series connected diode have been added to the primary side of a traditional push-pull converter. Table II contains the list of crucial simulation parameters.

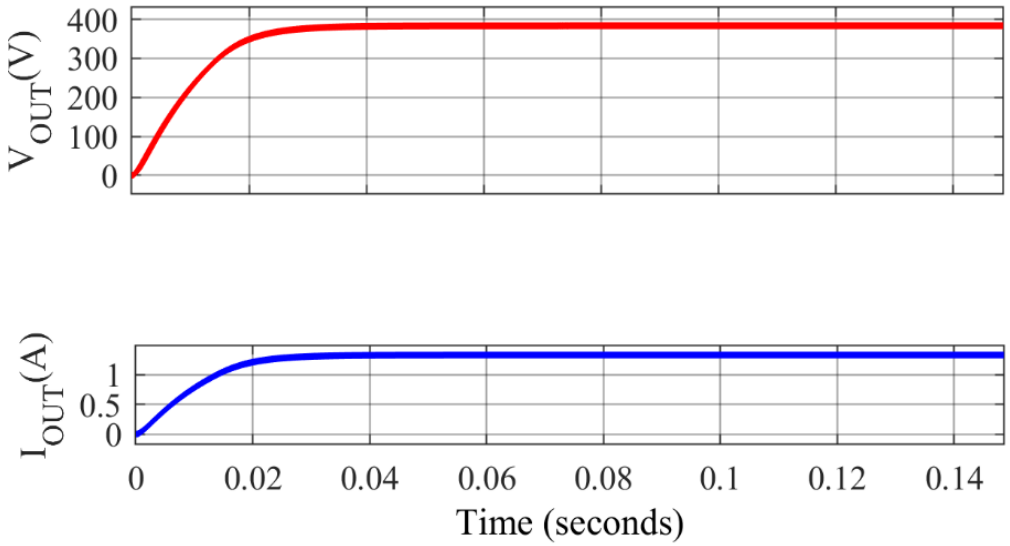

Fig. 4.4 Output Voltage $V_{OUT}(V)$ and Output Current $I_{OUT}(A)$

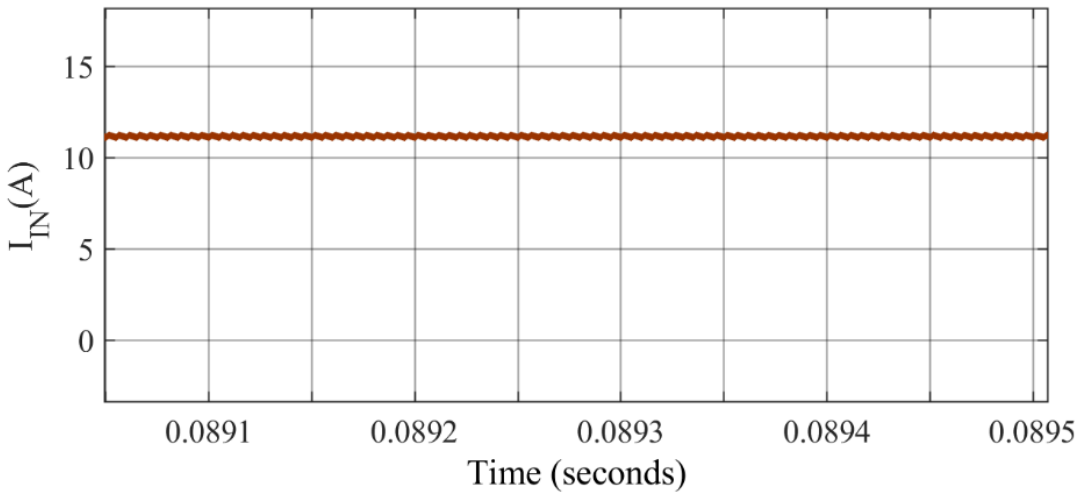

Fig. 4.5 Input Current $I_{IN}(A)$

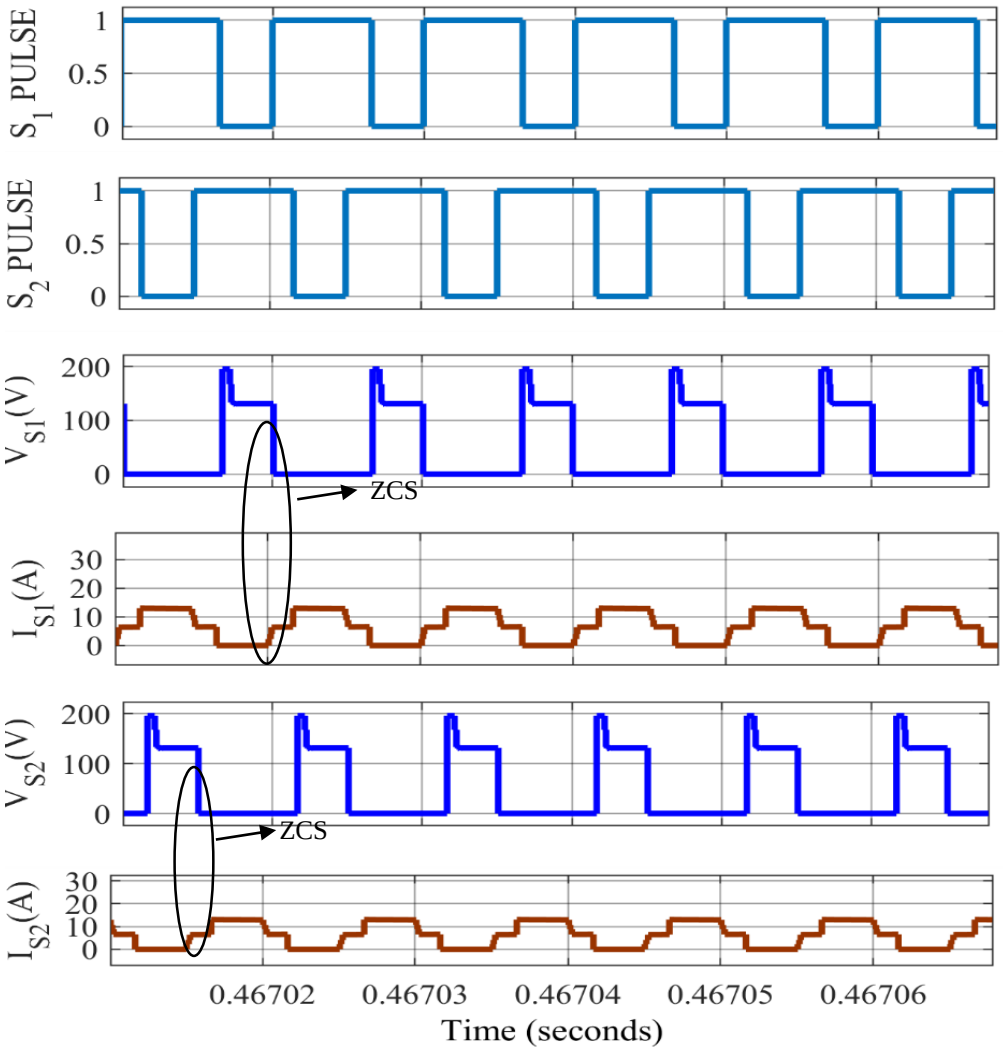

Fig. 4.6 S_1 and S_2 gate pulses with drain to source voltage and current

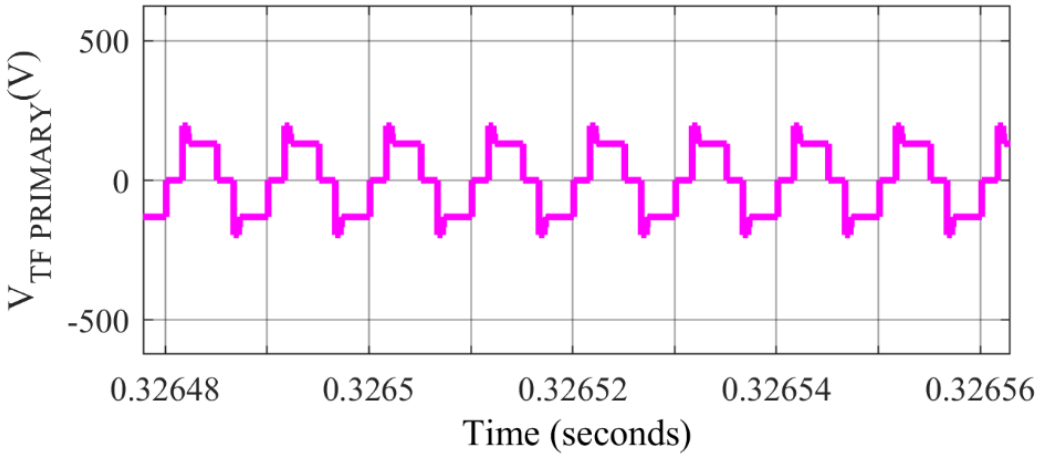

Fig. 4.7 Transformer primary voltages $V_{TF\ PRIMARY}\ (V)$

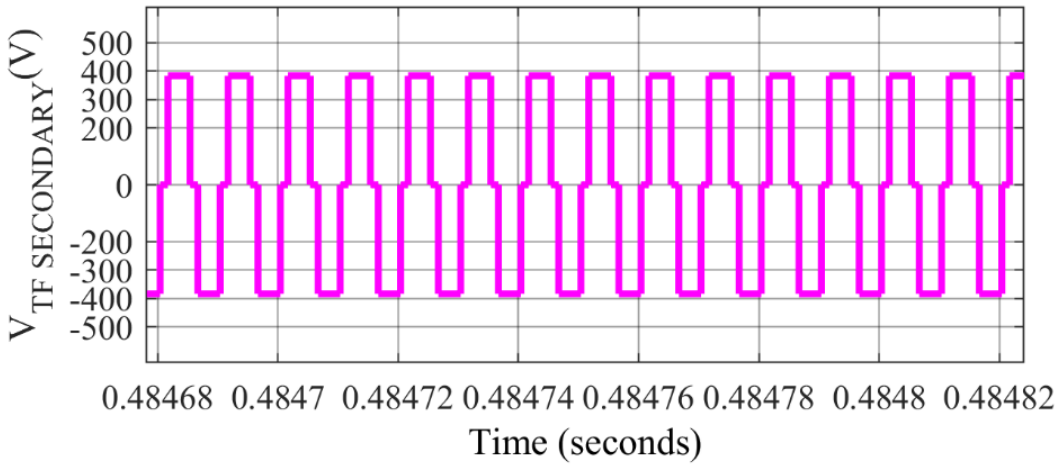

Fig. 4.8 Transformer secondary voltage $V_{TF\ SECONDARY}(V)$

Fig. 4.4 shows the output current and voltage waveforms. Because there is no overshoot or undershoot in the output waveforms, the settling time is reduced, and the required rating of the output capacitor is decreased, which lowers the overall cost. Due to the boost inductor's presence at the input, the maximum ripple current seen in Fig. 4.5 input current waveform is restricted to 0.5A and it also helps in boosting the voltage which in turn reduces the turn's ratio of the HF transformer resulting in reduction of size of the transformer. Fig. 4.6 displays the waveforms of the current and drain to source voltages for switches S_1 and S_2, in addition to the gating signals for each switch. As illustrated in Fig. 4.6, ZCS is obtained for switches S_1 and S_2 as a result of resonance between the primary side trapped capacitors and leakage inductance of the

HF transformer. This lowers the conduction losses and increases efficiency. It can be observed that the voltage spike is significantly reduced and is well under permissible limit as compared to conventional current fed push pull converter. Fig. 4.7, respectively, shows the waveforms of the primary voltage of the HF transformer and it can be seen that the voltage spike has been reduced due to the resonance at the primary side switches. Fig. 4.8 shows the transformer's secondary voltage. As a result of the inclusion of quick recovery SiC diodes on the output side, also the problem of reverse recovery is solved.

4.6 Comparative Analysis

The switch current and drain to source voltage waveforms of the two topologies i.e. conventional current fed push pull converter and dual capacitor trapped ZCS push pull converter are compared in Fig. 4.9. As compared to conventional current fed push pull, the voltage stress on the switches is lower in case of dual capacitor trapped ZCS push pull converter due to the ZCS operations of both the primary side switches as shown in Fig. 4.9. The proposed converter has lower voltage spike during switching as compared to conventional current fed push pull converter as shown in Fig. 4.9. The voltage spike is well under the permissible limit which helps in selecting the lower power rating switches. Fig. 4.10 represents the comparison between transformer's primary voltages for both topologies. The converter presented in this chapter features a quasi-square waveform at the transformer primary, which results in reduced losses in the transformer, less harmonics and less leakage flux, further leading to greater converter efficiency, as compared to topologies presented in chapter 3 depicted in Fig. 4.10. Fig. 4.11 represents the comparison between transformer's secondary voltages for both topologies and it can be seen that compared to conventional push pull converter the proposed converter has quasi-square waveform at transformer's secondary. The fast recovery SiC diodes present at the secondary side of the converter, minimizes the reverse recovery problem as compared to topology presented in chapter 3.

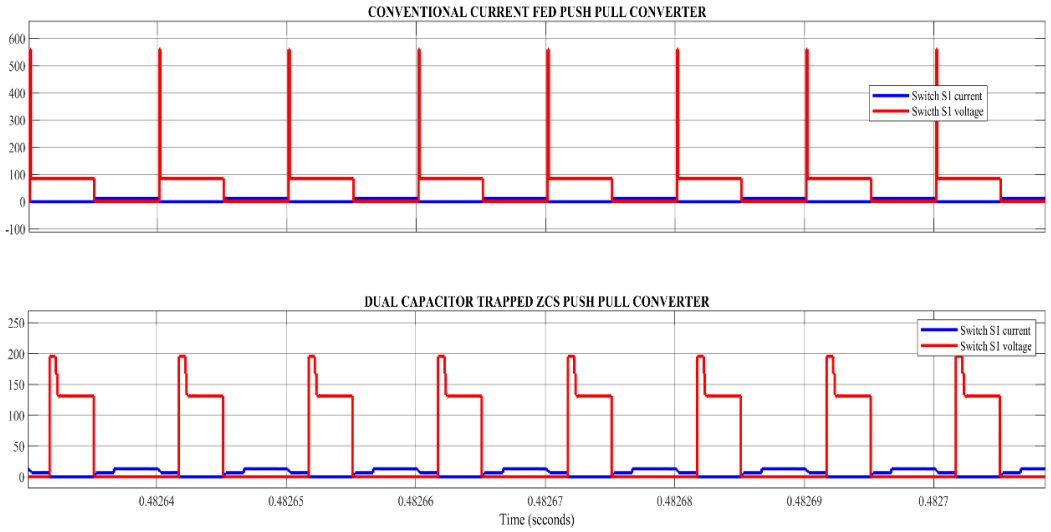

Fig. 4.9 Comparative waveform of switch current and voltage for Conventional current fed push pull converter VS Dual capacitor trapped push pull converter.

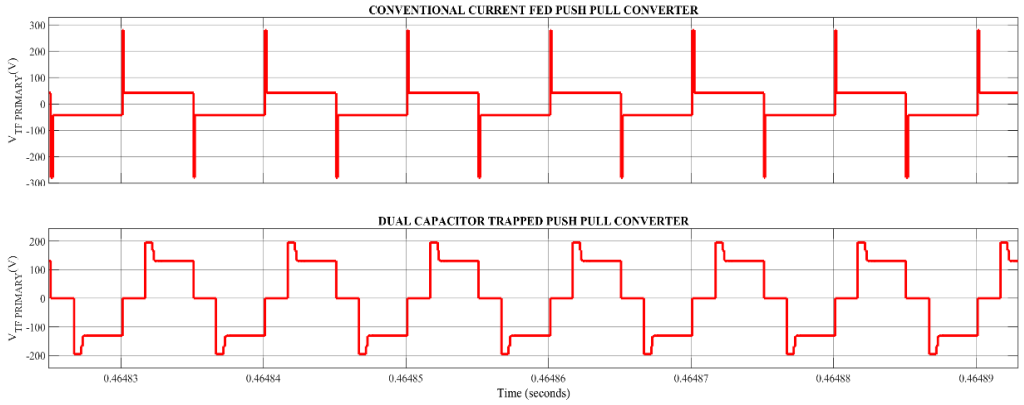

Fig. 4.10 Comparative waveform of Transformer primary voltage $V_{TF\ PRIMARY}\ (V)$ for Conventional current fed push pull converter VS Dual capacitor trapped push pull converter.

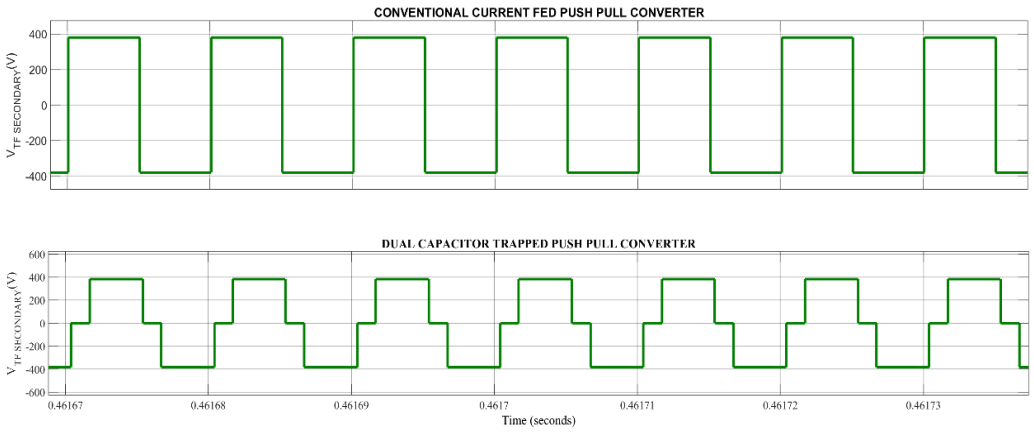

Fig. 4.11 Comparative waveform of Transformer secondary voltage $V_{TF\ SECONDARY}\ (V)$ for Conventional current fed push pull converter VS Dual capacitor trapped push pull converter.

CHAPTER 5
CAPACITOR TRAPPED ZCS PUSH PULL CURRENT FED CONVERTER FOR RENEWABLE ENERGY CONVERSION SYSTEM

5.1 Introduction

A new simple inherently clamped ZCS current-fed push–pull DC–DC converter for PV applications is proposed. The proposed converter includes a current-fed push–pull circuit with a trapped clamping capacitor, one HF transformer, a rectifier with fast-recovery SIC diodes and a capacitive filter to output power to 380V DC bus. ZCS turn off of primary switches are attained owing to the resonance between the trapped capacitor and the leakage inductance of the HF transformer, resulting in a near sinusoidal waveform at the primary of the HF transformer. The voltage spike across the power devices are suppressed effectively enabling the selection of low-voltage, low cost power devices. The proposed converter no auxiliary circuit is involved and since all the switches are ground referred, non-isolated driver with single power supply can be employed with very simple control. The power range of the proposed converter is 3KW. A 500W scaled down model was implemented in this chapter. The chapter briefly analysis and design the key characteristics and simulation results are discussed thereby demonstrating the capabilities of the converter in terms of boosting the voltage with desired power at high efficiency while undergoing ZCS operations.

5.2 System Configuration

The proposed converter configuration employs an inherently clamped ZCS operation of the 500W current fed push pull converter as shown in Fig. 5.1. The converter operates on low voltage DC bus duly fed by MPPT charge controller having voltage of 48V. The new configuration employ 2 blocking diodes with a trapped clamping capacitor on the primary side of conventional push pull converter which enable the configuration to achieve ZCS operation of the switches. The output side of the HF transformer is assumed connected with fast recovery SiC diodes to formulate a DC bus having output voltage 380V with a capacitive filter.

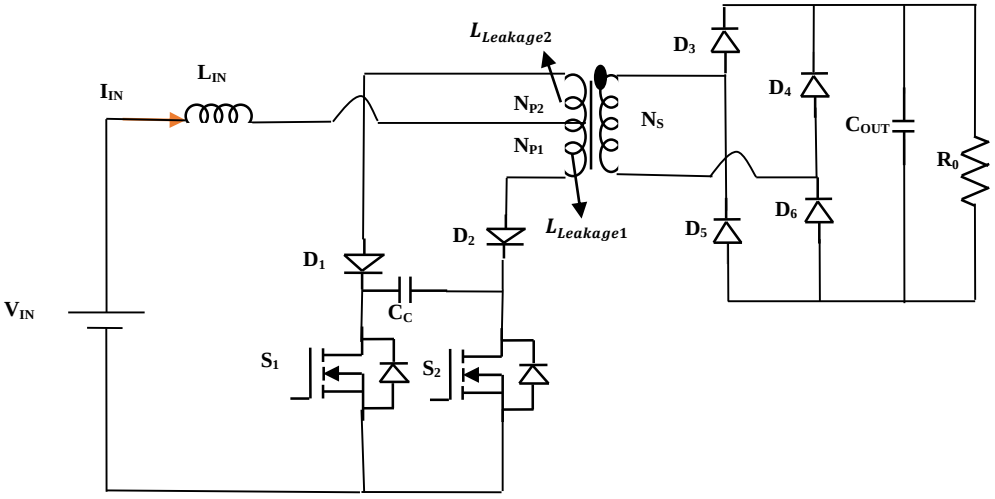

Fig. 5.1 Schematic of Proposed Converter

5.3 Modes of Operation

The proposed naturally clamped ZCS push pull converter's steady-state operation and analysis, together with pertinent mathematical equations and assumptions, is summarized in this section. The resonant tank for the ZCS functioning of the primary switches is composed of a trapped capacitor C_C and transformer leakage inductance $L_{Leakage}$. The gating signals of the switches have a duty cycle D that is larger than 50% and are 180 °phase-shifted. Fig. 5.2 shows the waveforms under steady conditions. The analysis was completed for the first half cycle, the intervals were repeated for the second half cycle with the other symmetrical devices conducting. Fig. 5.3 shows analogous circuits that represent the various operating modes of the converter.

The following presumptions are introduced in order simplify theoretical treatment.

1. The circuit operation is in a steady state.
2. The capacitance of the output capacitor C_{OUT} is sufficiently large, allowing the steady-state analysis to disregard output voltage ripple.
3. The duration of the commutation interval is very brief, resulting in negligible changes in both the transformer's magnetizing current and the input inductor current.
4. The windings in the transformer T are tightly coupled with one another,

and have negligibly small resistance.

5. The transformer operates symmetrically without bias magnetization.

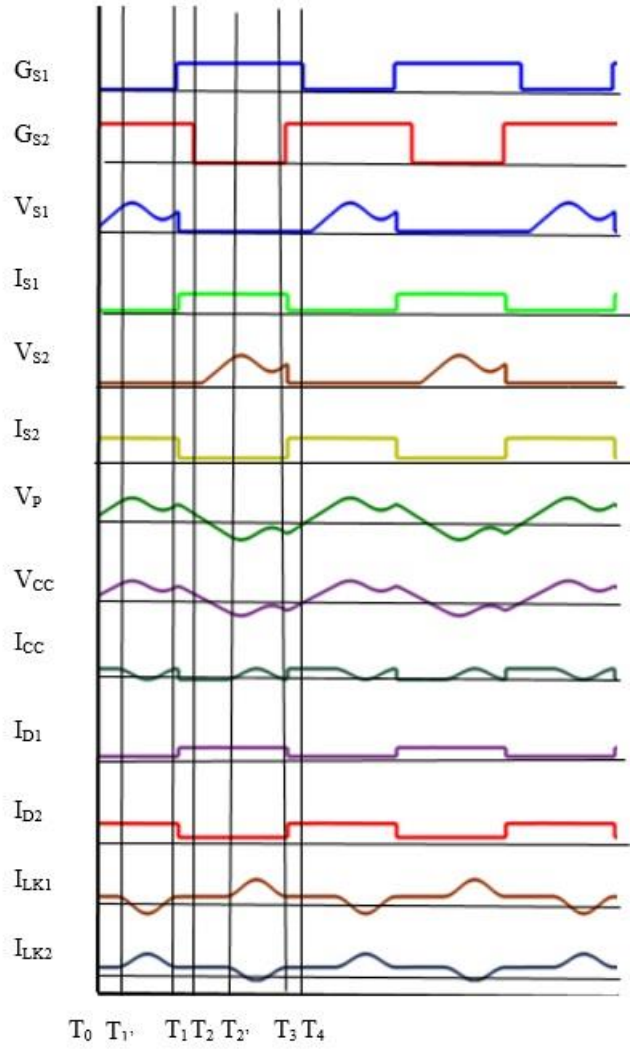

Fig 5.2 Switching pulses and steady state waveforms

A. Interval 1 (Fig. 5.2 : $T_0 < t < T_1'$) Mode 1(Fig. 5.3(a)):

In this interval the primary side switch S_2 is already and S_1 turns off conducting and diode D_3 and D_6 of secondary side rectifier bridge are conducting. Constant current I_{IN} flows through $L_{Leakage1}$ and $L_{Leakage2}$ of equal magnitude. Switch S_2 carries the entire input current. The trapped capacitor's voltage $V_{C\,trapped}$ is increasing until the capacitor gets charged and then the voltage is clamped at $2V_{P1}$.

$$V_{P1} = V_{P2} \tag{5.1}$$

$$V_{IN} = V_L + V_{P1} \tag{5.2}$$

$$V_{IN} = V_L - V_{P2} + V_{CC} \tag{5.3}$$

$$V_{P1} = \frac{V_{C\ trapped}}{2} \tag{5.4}$$

$$V_L = V_{IN} - \frac{V_{c\ trapped}}{2} \tag{5.5}$$

$$V_{C\ trapped} = 2V_{P1} \tag{5.6}$$

B. Interval 2 (Fig. 5.2 : $T_1' < t < T_1$) Mode 1(Fig. 5.3(a)):

The trapped capacitor starts discharging through the path: Trapped capacitor via Diode D_1 via S_1 parasitic capacitor to achieve turn ON of switch S_1. Current through $L_{Leakage1}$ starts decreasing sinusoidaly and current through $L_{Leakage2}$ starts increasing sinusoidaly.

C. Interval 3 (Fig. 5.2 : $T_1 < t < T_2$) Mode 3(Fig. 5.3(c)):

Switch S_1 is turned ON and all the primary side switches conduct simultaneously during this interval. The current through S_2 decreases and current through S_1 increases. The input current gets distributed in both primary leakage inductors due to the presence of clamping capacitor. Polarity across the capacitor got interchanged which signifies that the capacitor starts discharging which is supported by previous mode. Therefore ZCS turn OFF of S_2.

D. Interval 4 (Fig. 5.2 : $T_2 < t < T_2'$) Mode 2(Fig. 5.3(b)):

At T_2 the switch S_2 gets turned OFF and only S_1 is conducting diode D_5 and D_4 of secondary side rectifier bridge are conducting. Constant current I_{IN} flows through $L_{Leakage1}$ and $L_{Leakage2}$ of equal magnitude. Switch S_1 carries the entire input current. The trapped capacitor's voltage $V_{C\ trapped}$ is decreased until capacitor voltage is

clamped at $-2V_{P1}$.

E. Interval 5 (Fig. 5.2 : T_2' <t< T_3) Mode 2(Fig. 5.3(b)):

At T_2' current through $L_{Leakage1}$ starts increasing sinusoidaly and current through $L_{Leakage2}$ starts decreasing sinusoidaly and trapped capacitor C_C starts charging until it reaches its maximum value.

F. Interval 6 (Fig. 5.2 : T_3 <t< T_4) Mode 3(Fig. 5.3(c)):

Switch S_2 is turned ON and all the primary side switches conduct simultaneously during this interval. The current through S_1 decreases and current through S_2 increases. The input current gets distributed in both primary leakage inductors due to the presence of clamping capacitor. Polarity across the capacitor got interchanged which signifies that the capacitor starts discharging which is supported by previous mode. Therefore ZCS turn OFF for switch S_1 gets achieved.

$$V_{IN} = -V_L - V_{P1} + V_{CC} \tag{5.7}$$

$$V_{P1} = \frac{V_{C\ trapped}}{2} \tag{5.8}$$

$$V_L = \frac{V_{c\ trapped}}{2} - V_{IN} \tag{5.9}$$

$$V_{C\ trapped} = -2V_{P1} \tag{5.10}$$

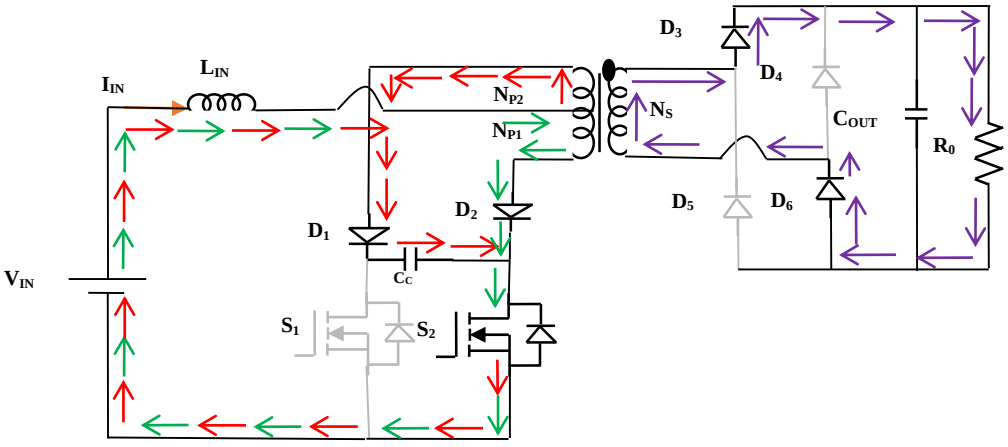

Fig. 5.3(a) Modes of Operations (Mode 1)

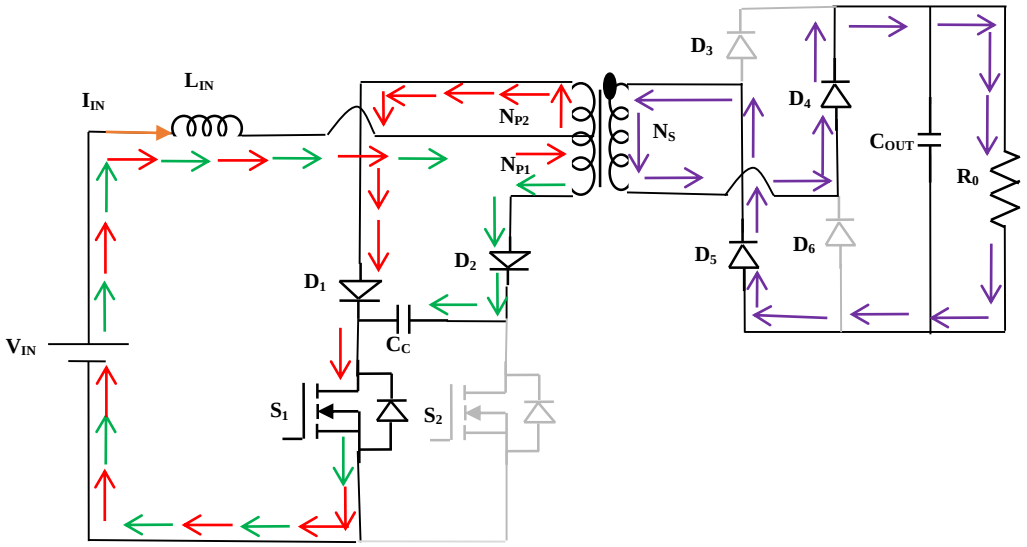

Fig. 5.3(b) Modes of Operations (Mode 2)

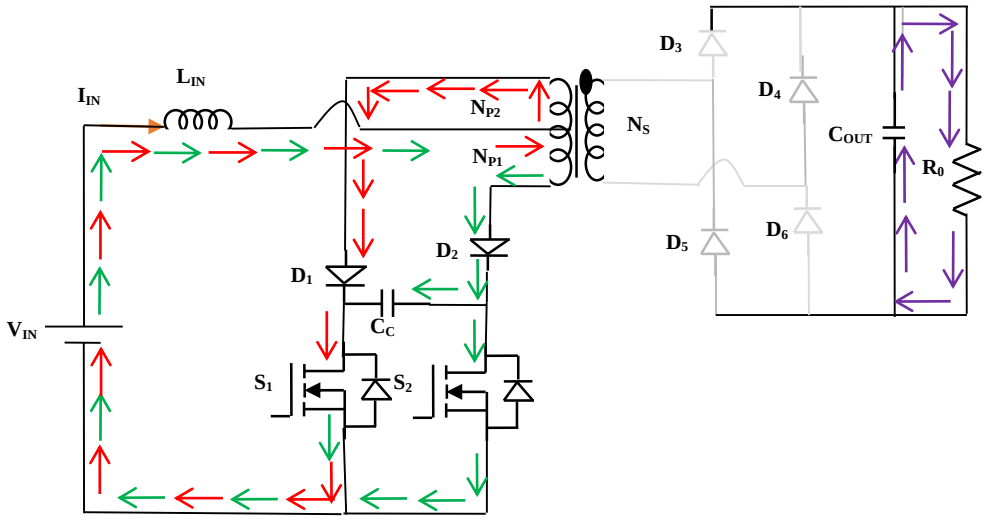

Fig. 5.3(c) Modes of Operations (Mode 3)

5.4 Mathematical Analysis

This work explains the analysis of the capacitor trapped ZCS current fed push-pull converter shown in Fig. 5.1. The notable characteristics of this converter include high efficiency, ZCS, component reduction, low cost and a low switching surge. In addition, the inductor's series connection with the input power source results in the suppression of backward noise and high immunity against external noise. Two operating modes are

analyzed in this study: the first when the switch S_1 or S_2 is ON, and the other when both switches S_1 and S_2 are ON. Second, the effects of the transformer's leakage inductance and trapped capacitor were discussed in detail. The formulation of differential equations that reflect the low-frequency behavior of the resonant converter is the initial step in the analytical process. Differential equations are derived in this analysis, and a few analytical expressions are explained. Calculations of the static and dynamic properties are also discussed. Our mathematical model considers the effects of the inductance of the transformer and trapped capacitor. Resistances against parasites were disregarded. Diodes are considered ideal for the analysis.

$V_{IN}(t)$: Input Voltage
$V_{DS1}(t)$,$V_{DS2}(t)$: Drain to Source Voltage of Mosfet Switch S_1 and S_2 respectively
$V_{C\ trapped}(t)$: Voltage across trapped capacitor
$I_{IN}(t)$: Input inductor current
$I_{OUT}(t)$: Output current
$V_{OUT}(t)$: Output Voltage
L_{TF}: Total leakage inductance of transformer's primary

A. State 1: When either S_2 or S_1 is ON

The circuit equations in this interval are:

$$V_{IN} = L_{IN}\frac{di}{dt} + \frac{d\emptyset}{dt} \tag{5.11}$$

Where ∅ is linkage flux associated with primary winding of the transformer.

$$I_{C\ trapped} = C_{trapped}\frac{dV_{C\ trapped}}{dt} \tag{5.12}$$

$$(I_{IN} - I_{C\ trapped}) - I_{C\ trapped} - nI_{OUT} = \frac{\emptyset}{L_{TF}} \tag{5.13}$$

$$V_{C\ trapped} = 2\frac{d\emptyset}{dt} \tag{5.14}$$

$$C_{OUT}\frac{dV_{OUT}}{dt}+\frac{V_{OUT}}{R}=I_{OUT} \tag{5.15}$$

Where n is turns ratio of transformer

$$n=\frac{N_2}{N_1} \tag{5.16}$$

Equation (5.13) represents the relation of transformers magnetizing current and linkage flux. By using Laplace transform technique to solve equation (5.11) to (5.15) we get

$$\emptyset(t)=\emptyset(0)+A\left(t-\frac{\sin w_0 t}{w_0}\right)+\frac{B}{w_0}(1-\cos w_0 t) \tag{5.17}$$

$$I_{IN}(t)=I_{IN}(0)+\frac{V_{IN}(t)}{L_{IN}}-\frac{A}{L}\left(t-\frac{\sin w_0 t}{w_0}\right)-\frac{B}{w_0 L_{IN}}(1-\cos w_0 t) \tag{5.18}$$

$$\begin{aligned}V_{OUT}(t)=V_{OUT}(0)&\left(1-\frac{t}{C_{OUT}R}-\frac{t^2}{2C_{OUT}}\right)+\frac{I_{OUT}(0)t}{C_{OUT}}\\&-\frac{nAC_{OUT}R^2}{1+(w_0C_{OUT}R)^2}\left[1-\frac{t}{C_{OUT}R}-\frac{{w_0}^2t^2}{2}\right.\\&\left.-\cos w_0t+\frac{\sin w_0t}{w_0C_{OUT}R}\right]\\&+\frac{nBC_{OUT}R^2}{1+(w_0C_{OUT}R)^2}\left[\frac{1}{w_0C_{OUT}R}+w_0t\right.\\&\left.-\frac{\cos w_0t}{w_0C_{OUT}R}-\sin w_0t\right]\end{aligned} \tag{5.19}$$

$$V_{C\,trapped}(t)=2A(1-\cos w_0 t)+2B\sin w_0 t \tag{5.20}$$

Where,$\emptyset(0)$, $I_{IN}(0)$, $V_{OUT}(0)$, $I_{OUT}(0)$ are initial values in this interval and the resonance frequency w_0 and parameters A and B are:

$$w_0=\frac{1}{2}\sqrt{\frac{1}{C_{trapped}}\left(\frac{1}{L_{TF}}\right)} \tag{5.21}$$

$$A = \frac{V_{IN} + nV_{OUT}L}{4{w_0}^2 LC_{trapped}} \tag{5.21}$$

$$B = \frac{I_{IN}(0) - nI_{OUT}(0) - \frac{\emptyset(0)}{L_{TF}}}{4w_0 C_{trapped}} \tag{5.22}$$

This state shifts to next state when the resonance voltage $V_{C\,trapped}$ reaches to zero.

B. State 2: When S1 and S2 both on

From the above equivalent circuit we get:

$$V_{IN} = L_{IN}\frac{di}{dt} \tag{5.23}$$

$$C_{OUT}\frac{dV_{OUT}}{dt} + \frac{V_{OUT}}{R} = 0 \tag{5.24}$$

Using Laplace transform,

$$\emptyset(t) = \emptyset(t1) \tag{5.25}$$

$$I_{IN}(t) = \frac{V_{IN}}{L_{IN}}(t - t_1) \tag{5.26}$$

$$V_{OUT}(t) = V_{OUT}(t1)\left(1 - \frac{t - t_1}{C_{OUT}R}\right) \tag{5.27}$$

Where t_1 is the time when both switches S_1 and S_2 are ON.

Putting the differentiation in the above differential equations and to be zero static characteristics are derived.

$$2\emptyset = A\left(t - \frac{\sin w_0 t}{w_0}\right) + \frac{B}{w_0}(1 - \cos w_0 t) \tag{5.28}$$

$$V_{IN}T_S = A\left(t - \frac{\sin w_0 t}{w_0}\right) + \frac{B}{w_0}(1 - \cos w_0 t) \tag{5.29}$$

$$V_{OUT}T_S = nA\left(t - \frac{\sin w_0 t}{w_0}\right) + \frac{nB}{w_0}(1 - \cos w_0 t) \tag{5.30}$$

Where $\emptyset$ is linkage flux and T_S is the switching period of the converter operation.

Above equations yields the following results

$$|\emptyset| = \frac{1}{2} V_{IN} T_S \tag{5.31}$$

$$V_{OUT} = nV_{IN} \tag{5.32}$$

Maximum value $V_{C\ (trapped\ \max)}$ of the resonance voltage is derived from the equation (5.20) as follows:

$$V_{C\ trapped\ ,max} = 2A + 2\sqrt{A^2 + B^2} \tag{5.33}$$

TABLE III SIMULATION PARAMETERS

Parameter	**Values**
Input voltage	48 V
Output voltage	380 V
Output power	500 W
Switching frequency	100 kHz
Turns Ratio	1:1:4.3
Leakage inductance ($L_{leakage1}$and $L_{leakage2}$ **)**	2 μH
Inductance of boost inductor	500 μH
Trapped capacitor (C_C)	50 nF
Output capacitor	220 μF

5.5 Simulation Results

The circuit of the proposed capacitor trapped ZCS push pull converter is implemented in MATLAB Simulink to verify the theoretical analysis. The converter is tested with a 48V DC input voltage with a 100 kHz switching frequency. 380V and 500W are the

specified output voltage and power, respectively. The Duty D at the specified input voltage is obtained as 0.58. The leakage inductance $L_{Leakage1}$ and $L_{Leakage2}$ of the transformer T, which has no air gaps, is 2µH. By using a boost inductor L_{IN} of 500µH, the maximum ripple current ΔI_{IN}, max is set to 0.3A at D 0.58. Two blocking diodes with a trapped capacitor C_C has been added on the primary side of conventional push pull converter to achieve ZCS. The voltage across the trapped capacitor is chosen from the circuit analysis presented above. The critical simulation parameters are listed in the Table III.

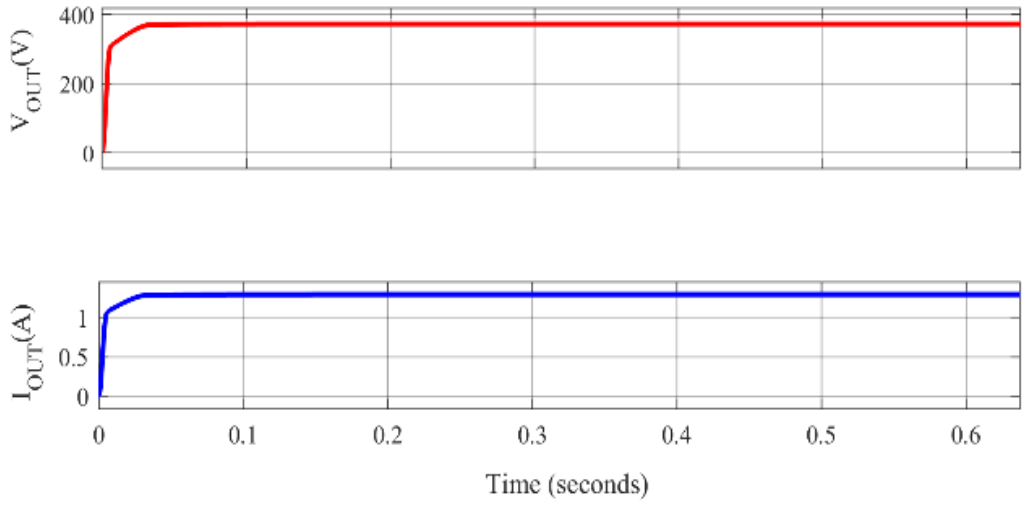

Fig. 5.4 Output Voltage $V_{OUT}(V)$ and Output Current $I_{OUT}(A)$

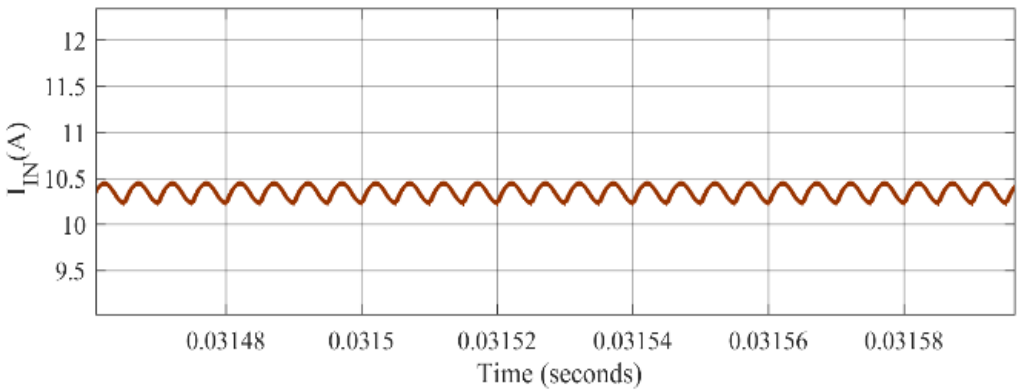

Fig. 5.5 Input Current $I_{IN}(A)$

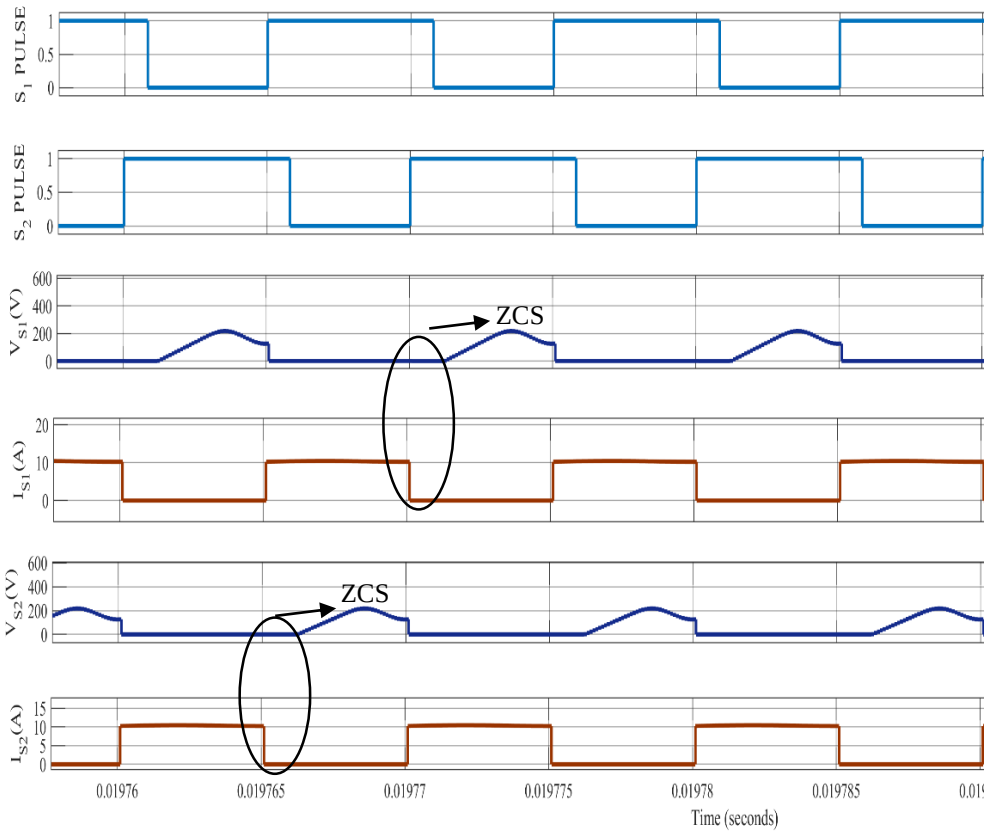

Fig. 5.6 S_1 and S_2 gate pulses with drain to source voltage and current

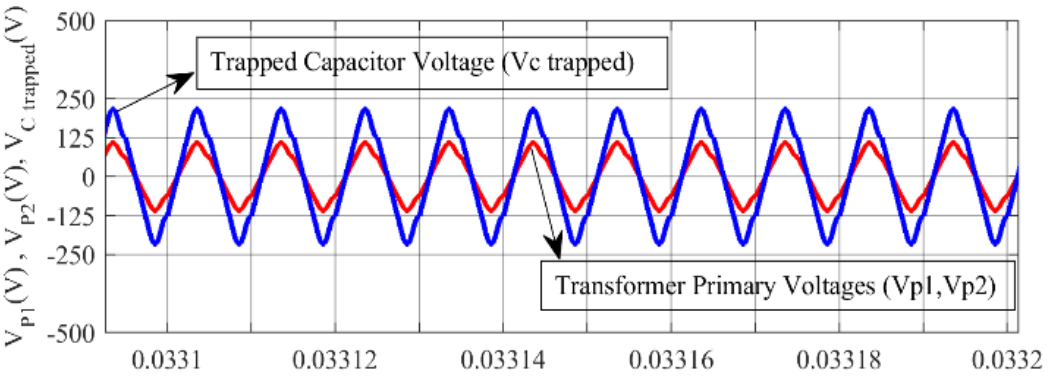

Fig. 5.7 Transformer primary voltages $V_{P1}(V)$and $V_{P2}(V)$ with Trapped Capacitor voltage $V_{C\ trapped}\ (V)$

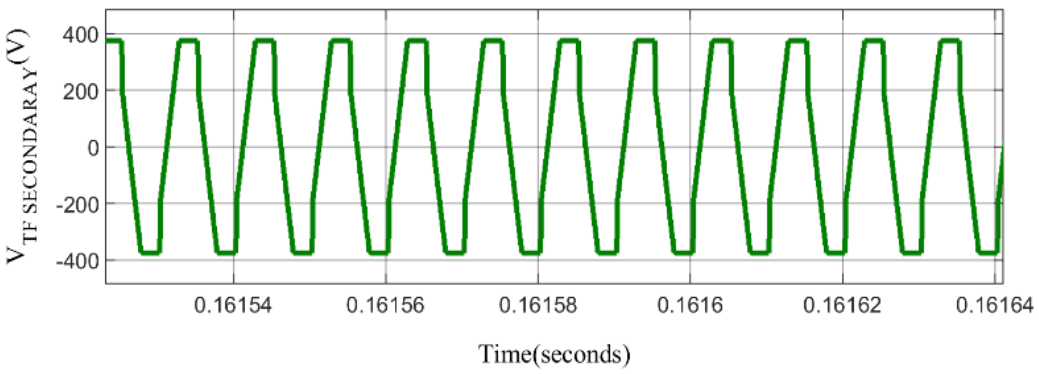

Fig. 5.8 Transformer secondary voltage $V_{TF\ SECONDARY}(V)$

Fig. 5.4 displays the output current and voltage waveforms measured at a 48V input and a 500W load condition. Fig. 5.4 shows that due to the presence of capacitive output filter the maximum output voltage ripple is 0.5V. Due to the boost inductor's presence at the input, the maximum ripple current seen in Fig. 5.5 input current waveform is restricted to 0.3A. In addition to the gating signals for switches S_1 and S_2, Fig. 5.6 shows the waveforms of the current and drain to source voltage for S_1 and S_2, respectively. ZCS are obtained for switches S_1 and S_2, respectively, as shown in Fig. 5.6 which eliminates the switching conduction losses hence increasing efficiency. Fig. 5.7, respectively, shows the waveforms of the trapped capacitor voltage and the primary voltages (V_{P1} and V_{P2}) of the transformer. Resonance on the primary side of the transformer causes a voltage waveform with a sinusoidal shape at the primary. It is clear that the trapped capacitor voltage is double the primary voltages of the transformer, as determined in the analytical section. As a result of the inclusion of quick recovery SiC diodes on the output side, reverse recovery problem is minimized. Fig. 5.8 shows the transformer's secondary voltage waveform which is near to sinusoidal wave shape.

5.6 Comparative Analysis

The switch current and drain to source voltage waveforms of the three topologies i.e. conventional current fed push pull converter, dual capacitor trapped ZCS push pull converter and capacitor trapped ZCS push pull converter are compared in Fig. 5.9. As compared to conventional current fed push pull and dual capacitor trapped push pull,

along with high voltage conversion ratio, the voltage stress on the switches is lowest in case of capacitor trapped ZCS push pull converter due to the ZCS operations of both the primary side switches as shown in Fig. 5.9.The proposed converter has no voltage spike during switching as compared to topologies presented in chapter 3 and chapter 4 as shown in Fig. 5.9. Also switch's drain to source voltage of the converter presented in this chapter is sinusoidal in shape as compared to other two topologies due to which the rating required of the power switches reduces. Fig. 5.10 represents the comparison between transformer's primary voltages for all three topologies. The converter presented in this chapter features a sinusoidal waveform at the transformer primary, which results in reduced losses in the transformer and less leakage flux, further leading to greater converter efficiency, as compared to topologies presented in chapter 3 and chapter 4 depicted in Fig. 5.10. Due to the sinusoidal waveform at the transformer's primary the harmonic losses also reduced. Fig. 5.11 represents the comparison between transformer's secondary voltages for all three topologies. As compared to topologies presented in chapter 3 and chapter 4 the efficiency of the converter proposed in this chapter is highest. Number of components required is reduced as compared to conventional current fed push pull converter. Only single gate driver is required as all the switches the ground referred. No auxiliary circuit is required for clamping of voltage as compared to conventional current fed push pull converter.

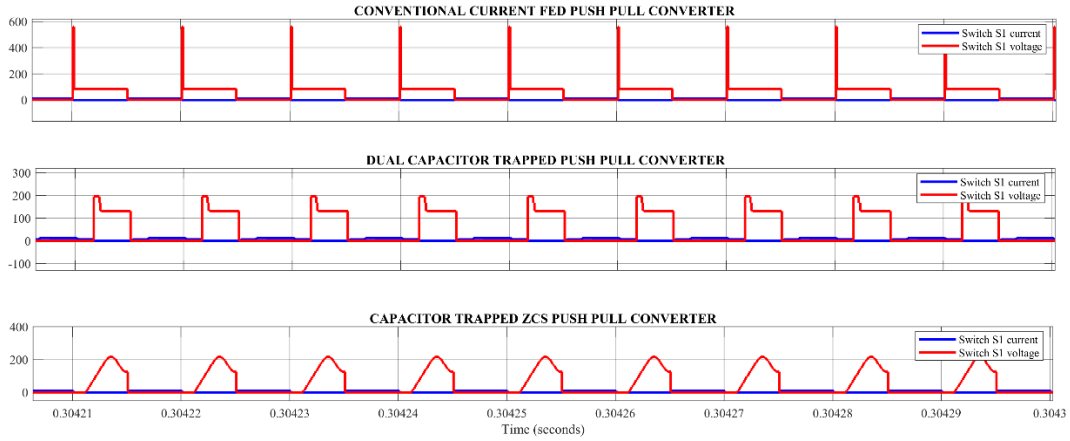

Fig. 5.9 Comparative waveform of switch current and voltage for Conventional current fed push pull converter VS Dual capacitor trapped push pull converter VS Capacitor trapped ZCS push pull converter

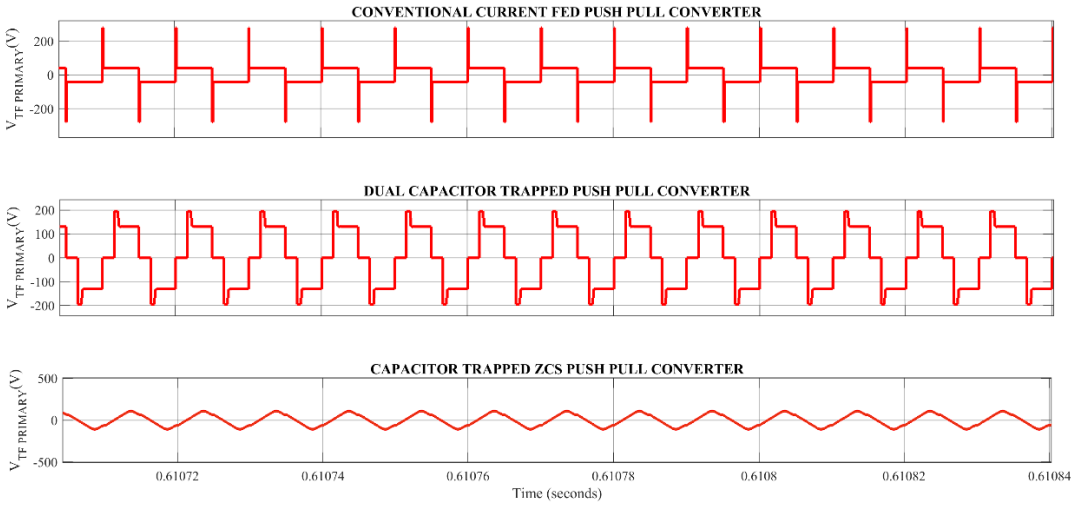

Fig. 5.10 Comparative waveform of Transformer primary voltage $V_{TF\ PRIMARY}\ (V)$ for Conventional current fed push pull converter VS Dual capacitor trapped push pull converter VS Capacitor trapped ZCS push pull converter

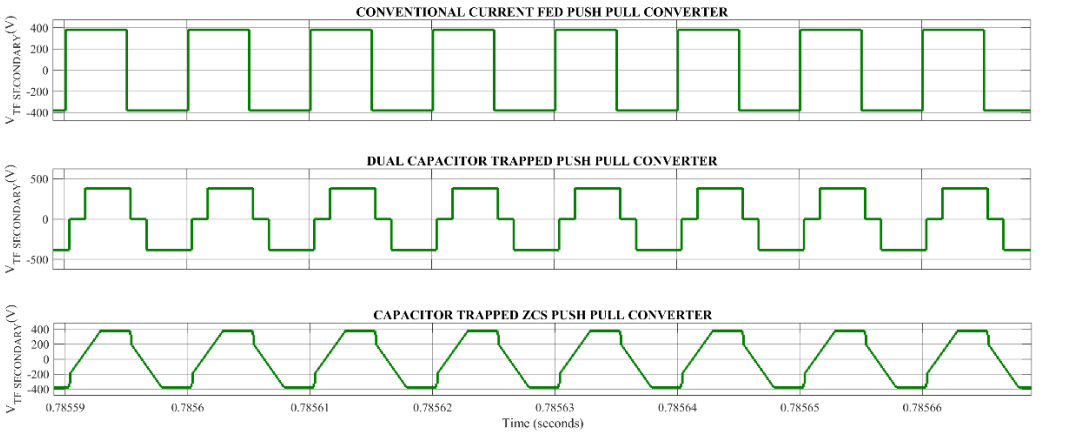

Fig. 5.11 Comparative waveform of Transformer secondary voltage $V_{TF\ SECONDARY}\ (V)$ for Conventional current fed push pull converter VS Dual capacitor trapped push pull converter VS Capacitor trapped ZCS push pull converter

CHAPTER 6
MAJOR CONCLUSIONS AND FUTURE SCOPE

6.1 Conclusion

In this thesis two capacitor trapped current fed push pull converters has been proposed. The analysis, design, and simulation results for the proposed converters have been showcased. High voltage conversion ratio, reduced switch conduction loss, and other features of the typical current fed push-pull converter are all preserved in the proposed converters. Moreover, the proposed converters outperforms all other examined topologies with an efficiency of 95.85% and 97.135% respectively. The proposed converter is suitable for the high step-up converter in fuel cells and solar cell applications due to its distinctive features like:

1) Soft switching which is accomplished due to the resonance between the trapped capacitor and leakage inductance of the HF transformer resulting in lower stress on the primary switches of the converter which enables the selection of low voltage , low power switches.

2) No auxiliary clamping circuit due to the natural clamping owing to the resonance between the HF leakage inductance and trapped capacitor.

3) Lesser components as no extra auxiliary circuit is required to achieve clamping.

4) Sinusoidal shape voltage waveform at the transformer primary owing to which the higher order harmonics in the transformers are reduced as a result the efficiency of the converter is improved,

5) Reverse recovery problem at the output side is minimized due to the selection of SiC diodes.

6) Low EMI noise owing to the sinusoidal voltage waveform at transformer primary which mitigate the higher order harmonics and result in lower EMI.

7) Higher Efficiency due to the reduction in conduction losses in the primary

switches as a result of soft switching.

8) Simple gate driver circuitry is required as all the switches are ground referred.

9) Higher reliability due to simple gate drive circuitry, no requirement of additional snubber circuit, low EMI and alleviation of stress on transformer.

6.2 Future Scope

1) Real time implementation.

2) The proposed converters can be utilized for bidirectional application.

3) Can be used as module integrated converter for high power application.

4) Higher order controller or nonlinear controller can be designed for the proposed converter.

REFERENCES

[1] Q. Wu, M. Wang, W. Zhou, C. Huang, G. Liu and X. Wang, "High Frequency Active-Clamped Zero-Current Switching Current-Fed Push-Pull Converter for Micro-Converter Applications," 2020 IEEE Energy Conversion Congress and Exposition (ECCE), Detroit, MI, USA, 2020, pp. 1273-1278, doi: 10.1109/ECCE44975.2020.9236043.

[2] K. R. Sree and A. K. Rathore, "Impulse Commutated Zero-Current Switching Current-Fed Push–Pull Converter: Analysis, Design, and Experimental Results," in IEEE Transactions on Industrial Electronics, vol. 62, no. 1, pp. 363-370, Jan. 2015, doi: 10.1109/TIE.2014.2331029.

[3] Qunfang Wu, Qin Wang, Jialin Xu, Zilong Xu, "Active-clamped ZVS current-fed push–pull isolated dc/dc converter for renewable energy conversion applications"in IET Power Electronics,Nov. 2017, doi: 10.1049/iet-pel.2017.0144.

[4] P. Xuewei and A. K. Rathore, "Naturally Clamped Zero-Current Commutated Soft-Switching Current-Fed Push–Pull DC/DC Converter: Analysis, Design, and Experimental Results," in IEEE Transactions on Power Electronics, vol. 30, no. 3, pp. 1318-1327, March 2015, doi: 10.1109/TPEL.2014.2315834.

[5] L. Jiang et al., "A New Push-Pull DC/DC Converter Topology With Complementary Active Clamped," in IEEE Transactions on Industrial Electronics, vol. 69, no. 6, pp. 6445-6449, June 2022, doi: 10.1109/TIE.2021.3088357.

[6] QUN Z., LEE F.C.: 'High-efficiency, high step-up DC–DC converters', IEEE Trans. Power Electron., 2003, 18,pp. 65– 73.

[7] E.-H. Kim, B.-H. Kwon, "High step-up resonant push–pull converter with high efficiency"in IET Power Electronics, June 2007, doi: 10.1049/iet-pel:20070140.

[8] O. Abdel-Rahim, A. Chub, A. Blinov and D. Vinnikov, "Current-Fed Dual Inductor Push-Pull Partial Power Converter," 2022 IEEE 20th International Power Electronics and Motion Control Conference (PEMC), Brasov, Romania, 2022, pp. 327-332, doi:10.1109/PEMC51159.2022.9962937.

[9] B. A. Basit, M. Kim and J. -W. Jung, "Improved Duty Compensation Control-Based Bidirectional Resonant DC–DC Converter with Reduced Input-Current Ripple for Battery Energy Storage Systems," in IEEE Transactions on Industrial Informatics, doi: 10.1109/TII.2023.3244349.

[10] J. M. Carrasco et al., "Power-Electronic Systems for the Grid Integration of Renewable Energy Sources: A Survey," IEEE Transactions on Industrial Electronics, vol. 53, no. 4, pp. 1002-1016, June 2006.

[11] M. Manojkumar, K. Porkumaran and C. Kathirvel, "Power electronics interface for hybrid renewable energy system — A survey," in 2014 International Conference on Green Computing Communication and Electrical Engineering (ICGCCEE), Coimbatore, 2014, pp. 1-9.

[12] P. V. Joshi, Y. S. Bhavsar, S. S. Dhamal, A. M. Lulhe and T. P. Pandhi, "Grid

interconnection of DC microgrid at distribution level using power electronic converter system-MATLAB/Simulink modeling and analysis," in 2016 International Conference on Automatic Control and Dynamic Optimization Techniques (ICACDOT), Pune, 2016, pp. 1056-1061.

[13] Kwon, B.H., Choi, J.H., Kim, T.W.: Improved single-phase line-interactive UPS. IEEE Trans. Ind. Electron. 48(4), 804–811 (2001)

[14] Yu, S., Nguyen, M.Q., Choi, W.: A novel soft-switching battery charge/discharge converter with the zero voltage discharge function.IEEE Trans. Power Electron. 31(7), 5067–5078 (2016).

[15] Pahlevaninezhad, M., Drobnik, J., Jain, P.K., Bakhashai, A.: A load adaptive control approach for a zero-voltage-switching dc/dc converter used for electric vehicles. IEEE Trans. Ind. Electron. 59(2), 920–933 (2012).

[16] Jin, K., Ruan, X.: Hybrid full-bridge three-level LLC resonant converter—a novel DC-DC converter suitable for fuel-cell power system. IEEE Trans.Ind. Electron. 53(5), 1492–1503 (2006).

[17] Zhang, J., Wu, H., Qin, X., Xing, Y.: PWM plus secondary-side phaseshift controlled soft-switching full-bridge three-port converter for renewable power systems. IEEE Trans. Ind. Electron. 62(11), 7061–7072 (2015).

[18] T.-F. Wu, Y.-C. Chen, J.-G. Yang, and C.-L. Kuo, “Isolated bidirectional full-bridge DC–DC converter with a flyback snubber,” IEEE Trans.Power Electron., vol. 25, no. 7, pp. 1915–1922, Jul. 2010.

[19] Y. Kim; I. Lee; I.Cho; G. Moon, “Hybrid dual full-bridge DC–DC converter with reduced circulating current, output filter, and conduction loss of rectifier stage for RF power generator application," IEEE Trans.Power Electron., vol.29, no.3, pp.1069-1081, March 2014.

[20] Corradini, L.,Seltzer, D., Bloomquist, D., Zane, R., Maksimović, D.,Jacobson, B., "Minimum Current Operation of Bidirectional Dual-Bridge Series Resonant DC/DC Converters", IEEE Trans. Power Electron.,vol.27, no.7, pp.3266-3276, July 2012.

[21] X. Li and A. K. S. Bhat, “Analysis and design of high-frequency isolated dual-bridge series resonant DC/DC converter,” IEEE Trans. Power Electron., vol. 25, no. 4, pp. 850–862, Apr. 2010.

[22] R.-J. Wai, C.-Y. Lin, and Y.-R. Chang, “High step-up bidirectional isolated converter with two input power sources,” IEEE Trans. Ind.Electron., vol. 56, no. 7, pp. 2629–2643, Jul. 2009.

[23] Lizhi Zhu, “A Novel Soft-Commutating Isolated Boost Full-bridge ZVS-PWM DC-DC Converter for Bi-directional High Power Applications,” IEEE Trans. Power Electron., vol. 21, no. 2, pp. 422–429, Mar. 2006.

[24] M. Delshad and H. Farzanehfard, "A soft switching flyback current-fed push pull Dc-Dc Converter with active clamp circuit," 2008 IEEE 2nd International Power and Energy Conference, Johor Bahru, Malaysia, 2008, pp. 203-207, doi: 10.1109/PECON.2008.4762471.

[25] S. Bal, A. K. Rathore and D. Srinivasan, "Naturally clamped snubberless soft-switching bidirectional current-fed three-phase push-pull DC/DC converter for DC micro-grid application," 2015 IEEE Applied Power Electronics Conference and Exposition (APEC), Charlotte, NC, USA, 2015, pp. 717-724, doi: 10.1109/APEC.2015.7104429.

[26] P. J. Barnawal, V. N. Lal and R. K. Singh, "Current-fed LLC Based Dual Half Active Bridge Resonant Converter," 2022 IEEE International Conference on Power Electronics, Drives and Energy Systems (PEDES), Jaipur, India, 2022, pp. 1-5, doi: 10.1109/PEDES56012.2022.10080558.

[27] M. Delshad and H. Farzanehfard, "A soft switching flyback current-fed push pull Dc-Dc Converter with active clamp circuit," 2008 IEEE 2nd International Power and Energy Conference, Johor Bahru, Malaysia, 2008, pp. 203-207, doi: 10.1109/PECON.2008.4762471.

[28] S. Sooksatra and W. Subsinaha, "Boost Derived Full-Bridge ZCS Resonant Converter Using Inductive Output Filter," 2022 International Power Electronics Conference (IPEC-Himeji 2022- ECCE Asia), Himeji, Japan, 2022, pp. 354-361, doi: 10.23919/IPEC-Himeji2022-ECCE53331.2022.9806926.

[29] S. . -Y. Tseng, Y. . -J. Li and Y. . -J. Wu, "Buck converter associated with active clamp flyback converter for PV power system," 2008 IEEE International Conference on Sustainable Energy Technologies, Singapore, 2008, pp. 916-921, doi: 10.1109/ICSET.2008.4747138.

[30] R. Y. Chen, R. L. Lin, T. J. Liang, J. F. Chen, and K. C. Tseng,"Current-fed full-bridge boost converter with zero current switching for high voltage applications," Fourtieth IAS Annual Meeting. Conference Record of the 2005 Industry Applications Conference, 2005, pp.2000-2006.

[31] Stanislaw Jalbrzykowski and Tadeusz Citko, "Current-Fed Resonant Full-Bridge Boost DC/AC/DC Converter," IEEE Trans. Ind. Electron.,vol. 55, no.3 ,pp.1198-1205, March 2008.

[32] Tsorng-Juu Liang; Ren-Yi Chen; Jiann-Fuh Chen; Wei-Jin Tzeng; ,"Buck-type current-fed push-pull converter with ZCS for high voltage applications," TENCON 2007 - 2007 IEEE Region 10 Conference, Oct.30 2007-Nov. 2 2007, pp.1-4.

[33] F. Krismer, J. Biela, and J.W. Kolar, "A comparative evaluation of isolated bi-directional DC/DC converters with wide input and output voltage range," Fourtieth IAS Annual Meeting in Industry Applications Conference, 2005, pp.599-606.

[34] M. Mohr and F.-W. Fuchs, "Voltage fed and current fed full bridge converter for the use in three phase grid connected fuel cell systems," in Proc. IEEE Int. Power Electron. Motion Control Conf., 2006, pp. 1–7.

[35] Akshay K Rathore and Prasanna UR, "Comparison of soft-switching voltage-fed and current-fed bi-directional isolated Dc/Dc converters for fuel cell vehicles," in Proc. IEEE ISIE, May 2012, pp. 252-257.

[36] R.-J. Wai, C.-Y. Lin, and Y.-R. Chang, "High step-up bidirectional isolated converter with two input power sources," IEEE Trans. Ind. Electron., vol. 56, no. 7, pp. 2629–2643, Jul. 2009.

[37] Lizhi Zhu, “A Novel Soft-Commutating Isolated Boost Full-bridge ZVS-PWM DC-DC Converter for Bi-directional High Power Applications,” IEEE Trans. Power Electron., vol. 21, no. 2, pp. 422–429, Mar. 2006.

[38] P. Xuewei and A. K. Rathore, “Novel Interleaved Bidirectional Snubberless Soft switching Current-fed Full-bridge Voltage Doubler for Fuel Cell Vehicles,” IEEE Transactions on Power Electronics, vol. 28, no. 12, Dec. 2013, pp. 5355-5546.

[39] A. K. Rathore and U. R. Prasanna, “Analysis, Design, and Experimental Results of Novel Snubberless Bidirectional Naturally Clamped ZCS/ZVS Current-fed Half-bridge Dc/Dc Converter for Fuel Cell Vehicles,” IEEE Trans. Ind. Electron., no.99, Aug. 2012.

[40] S. J. Jang, C. Y. Won, B. K. Lee and J. Hur, “Fuel cell generation system with a new active clamping current-fed half-bridge converter,” IEEE Trans. on Energy Conversion, vol. 22, no.2, pp. 332-340, June 2007.

[41] S. Han, H. Yoon, G. Moon, M. Youn, Y. Kim, and K. Lee, “A new active clamping zero-voltage switching PWM current-fed half bridge converter,” IEEE Trans. Power Electron., vol.20, no.6, pp 1271-1279, Nov.2006.

[42] Tsai-Fu Wu, Jin-Chyuan Hung, Jeng-Tsuen Tsai, Cheng-Tao Tsai, and Yaow-Ming Chen, “An active-clamp push-pull converter for battery sourcing application,” IEEE Trans. Industry Application., vol.44, no.1, pp.196-204, Jan.2008.

[43] C.L. Chu and C.H. Li, “Analysis and design of a current-fed zero-voltage-switching and zero-current-switching CL-resonant push-pull dc-dc converter,” IET Power Electron., vol. 2, no. 4, pp. 456–465, Jul. 2009.

[44] Tarzamni, H., Babaei, E., Esmaeelnia, F.P., Dehghanian, P., Tohidi, S.,Sharifian, M.B.B.: Analysis and reliability evaluation of a high step-up soft switching push–pull dc–dc converter. IEEE Trans. Relia. 69(4), 1376-1386 (2020).

[45] Larico, H.R.E., Barbi, I.,: Three-phase push-pull DC-DC converter: analysis, design, and experimentation. IEEE Trans. Ind. Electron. 59(12), 4629–4636 (2012).

[46] Zeljkovic, S., Reiter, T., Gerling, D.,: Efficiency optimized single-Stage reconfigurable DC/DC converter for hybrid and electric vehicles. IEEE J. Emerg. Sel. Top. Power Electron. 2(3), 496–506, (2014).

[47] Costa, A.E.L., Andersen, R.L.: High-gain three-phase current-fed push–pull DC–DC converter. IET Power Electron. 13(3), 545–556 (2020).

[48] Lee, S., Park, J., Choi, S.: A three-phase current-fed push–pull DC–DC converter with active clamp for fuel cell applications. IEEE Trans. Power Electron. 26(8), 2266–2277 (2011).

[49] Tandon, S., Rathore, A.K.: Analysis and design of series LC partialresonance pulse based ZCS current-fed push-pull converter. IEEE Trans.Ind. Appl. 57(4), 4232-4241 (2021).

[50] Pan, X., Akshay, K.R.: Naturally clamped zero-current commutated softswitching current-fed push–pull DC/DC converter: analysis, design,

andexperimental results. IEEE Trans. Power Electron. 30(3), 1318–1327(2015).

[51] R. Kosenko, A. Chub and A. Blinov, "Full-soft-switching high step-up bidirectional isolated current-fed push-pull DC-DC converter for battery energy storage applications," IECON 2016 - 42nd Annual Conference of the IEEE Industrial Electronics Society, Florence, Italy, 2016, pp. 6548-6553, doi: 10.1109/IECON.2016.7794014.

[52] Patwardhan, A.A., Deo, M.S., Mangal, M.: 18 kW DC-DC converter using push-pull inverter with lossless snubber circuits. Proc. Power Electron Drives Energy Syst. (PEDES) 2, 789-793 (1996).

[53] Bor-Ren Lin, Kevin Huang and David Wang, "Analysis, design, and implementation of an active clamp forward converter with synchronous rectifier," in IEEE Transactions on Circuits and Systems I: Regular Papers, vol. 53, no. 6, pp. 1310-1319, June 2006, doi: 10.1109/TCSI.2006.870900.

[54] S. Liu, H. Lin and T. Wang, "Comparative Study of Three Different Passive Snubber Circuits for SiC Power MOSFETs," 2019 IEEE Applied Power Electronics Conference and Exposition (APEC), Anaheim, CA, USA, 2019, pp. 354-358, doi: 10.1109/APEC.2019.8722302.

[55] M. Zarghani, S. Peyghami, F. Iannuzzo, F. Blaabjerg and S. Kaboli, "An Energy Recovery Scheme for RCD Snubber in the Series Configuration of IGBTs," 2021 IEEE Energy Conversion Congress and Exposition (ECCE), Vancouver, BC, Canada, 2021, pp. 5183-5189, doi: 10.1109/ECCE47101.2021.9595162.

[56] Ryan,M.J., Brumsickle,W.E., Divan,D.M., Lorenz, R.D.: A new ZVS LCLresonant push-pull DC-DC converter topology. IEEE Trans. Ind. Appl.34(5), 1164–1174 (1998).

[57] Yuan, Y., Wu, Q.: One zero-voltage-switching three-transistor push–pull converter. IET Power Electron. 6(7), 1270–1278 (2013).

[58] Chen, Z.,Wu,Q., Yuan, Y.: A novel zero-voltage-switching push–pull highfrequency-link single-phase inverter'. IEEE J. Emerg. Sel. Top. Power Electron.4(2), 421–434 (2016).

[59] Shoyama, M., Harada, K.: Zero-voltage-switching realized by magnetizing current of transformer in push–pull current-fed DC–DC. in Proceedings of Power Electron. Spec. Conf., (1993), 178–184.

[60] Xu, J., Wu, Q., Wang, Y.: Magnetising-current-assisted wide ZVS range push–pull DC/DC converter with reduced circulating energy. IET Power Electron., 11(2), 272-279 (2018).

[61] Y. Wei, Q. Luo, D. Woldegiorgis, H. Mhiesan and A. Mantooth, "Characteristics Analysis of LLC and LCL-T Resonant Tank," 2020 IEEE Transportation Electrification Conference & Expo (ITEC), Chicago, IL, USA, 2020, pp. 427-432, doi: 10.1109/ITEC48692.2020.9161709.

[62] Wei Chen and Zhengyu Lu, "A novel ZVS push-pull type LLC series resonant Dc-Dc converter for hybrid fuel cell power systems," 2008 IEEE Power Electronics Specialists Conference, Rhodes, Greece, 2008, pp. 1651-1656, doi: 10.1109/PESC.2008.4592178.

[63] Wu, Q., Wang, Q., Xu, J., Xiao, L.: Implementation of an active-clamped

current-fed push–pull converter employing parallel-inductor to extend ZVS range for fuel cell application. IEEE Trans. Ind. Electron. 64(10), 7919-7929 (2017).

[64] Wu, Q., Wang, Q., Xu, J., Xu, Z.: Active-clamped ZVS current-fed push–pull isolated dc/dc converter for renewable energy conversion applications.IET Power Electron. 11(2), 373–381 (2018).

[65] Torrico-Bascope, R., Antunes, F.L.M., Barbi, I.: Optimal double ZVSPWM active-clamping forward converter with inputs connected in series and parallel. in Proc. IEEE Power Electron. Spec. Conf. (APEC), (2004),1621–1626.

[66] Lim, J.W., Jamil, H., Kim, M.: Bidirectional soft switching push-pull resonant converter over wide range of battery voltages. IEEE Trans. Power Electron. 36(11), 12251-12267 (2021).

[67] Wu, T.F., Hung, J.C., Tsai, J.T., Tsai, C.T., Chen, Y.M.: An active-clamp push-pull converter for battery sourcing applications. IEEE Trans. Ind.Appl. 44(1), 196–204 (2008).

[68] L. Jiang et al., "A New Push-Pull DC/DC Converter Topology With Complementary Active Clamped," in IEEE Transactions on Industrial Electronics, vol. 69, no. 6, pp. 6445-6449, June 2022, doi: 10.1109/TIE.2021.3088357.

[69] Q. Wu, Q. Wang, J. Xu and L. Xiao, "A Wide Load Range ZVS Push–Pull DC/DC Converter With Active Clamped," in IEEE Transactions on Power Electronics, vol. 32, no. 4, pp. 2865-2875, April 2017, doi:10.1109/TPEL.2016.2577639.

LIST OF PUBLICATIONS

Paper	Author list . Title. Conference/Journal	Status
[1]	Dhananjay Yadav, Vishal Verma, **"Capacitor Trapped Current Fed ZCS-ZVS Push Pull DC-DC converter for renewable energy conversion"** 5th IEEE International Conference on Power Energy and Environment (ICEPE 2023)	Accepted
[2]	Dhananjay Yadav, Vishal Verma, **"Dual Capacitor Trapped Current Fed ZCS Push Pull DC-DC converter for renewable energy conversion"** International Conference on Power Electronics, Smart Grid, and Renewable Energy (PESGRE 2023)	Communicated